Ocean Science
Discussions

Open Access

EGU

Australian tidal currents – assessment of a barotropic model with an unstructured grid.

David A. Griffin[1], Mike Herzfeld[1], Mark Hemer[1]

[1]Oceans and Atmosphere, CSIRO, Hobart, TAS 7000, Australia

5 *Correspondence to*: David Griffin (David.Griffin@csiro.au)

Abstract. While the variations of tidal range are large and fairly well known across Australia (less than 1 m near Perth but more than 14 m in King Sound), the properties of the tidal currents are not. We describe a new regional model of Australian tides and assess it against a validation dataset comprising tidal height and velocity constituents at 615 tide gauge sites and 95 current meter sites. The model is a barotropic implementation of COMPAS, an unstructured-grid primitive-equation model

10 that is forced at the open boundaries by TPXO9v1. The Mean Absolute value of the Error (MAE) of the modelled M2 height amplitude is 9.3 cm, or 13 % of the 73 cm mean observed amplitude. The MAE of phase (11°), however, is significant, so the M2 Mean Magnitude of Vector Error (MMVE, 20 cm) is significantly greater. Results for 5 other major constituents are similar. We conclude that while the model has skill at height in all regions, there is definitely room for improvement (especially at some specific locations) before harmonic predictions based on observations are rendered obsolete. For the M2 major-axis

15 velocity amplitude, the MAE across the 95 current meter sites, where the observed amplitude ranges from 0.1 cm s^{-1} to 144 cm s^{-1}, is 6.5 cm s^{-1}, or 20 % of the 31.7 cm s^{-1} observed mean. This nationwide average result is not much greater than the equivalent for height, but it conceals a larger regional variation. Relative errors on the narrow shelves of NSW and Western Australia exceed 100 %, but tidal currents are weak and negligible there compared to non-tidal currents. We show that the model has predictive value for much of the 79 % of Australia's shelf seas where tides are a major component of the total

20 velocity variability. In descending order this includes the Bass Strait, Kimberley to Arnhem Land and Southern Great Barrier Reef regions. There is limited evidence the model is also valuable for currents in other regions across northern Australia. We plan to commence publishing 'unofficial' tidal current predictions for chosen regions in the near future, based on both the limited number of observations, and the COMPAS model.

1 Introduction

25 Tidal currents are a major component of the velocity variability for most of the Australian continental shelf, yet tidal current predictions are only listed in the Australian National Tide Tables for 7 sites, 5 of which are in Torres Strait. As part of a project to map Australia's tidal energy resource, and as a step towards an operational, model-based tidal current forecasting ability, we have compiled a tidal currents harmonic constituents validation dataset at 95 sites based on observations acquired by a number of agencies. This is a significant number of sites, but it is still small compared to the 683 sites for which the Bureau of

30 Meteorology Tidal Unit has estimates of tidal height harmonic constituents. We use these validation datasets for currents and

heights to assess the errors of a newly configured barotropic implementation of an unstructured-grid tidal model for the Australian continental shelf. This tells us how well the tidal component of the total variability can be predicted. Taking non-tidal currents into account as well, we identify the regions of Australia where model-based tidal current predictions are not only accurate, but also a large part of the total variability.
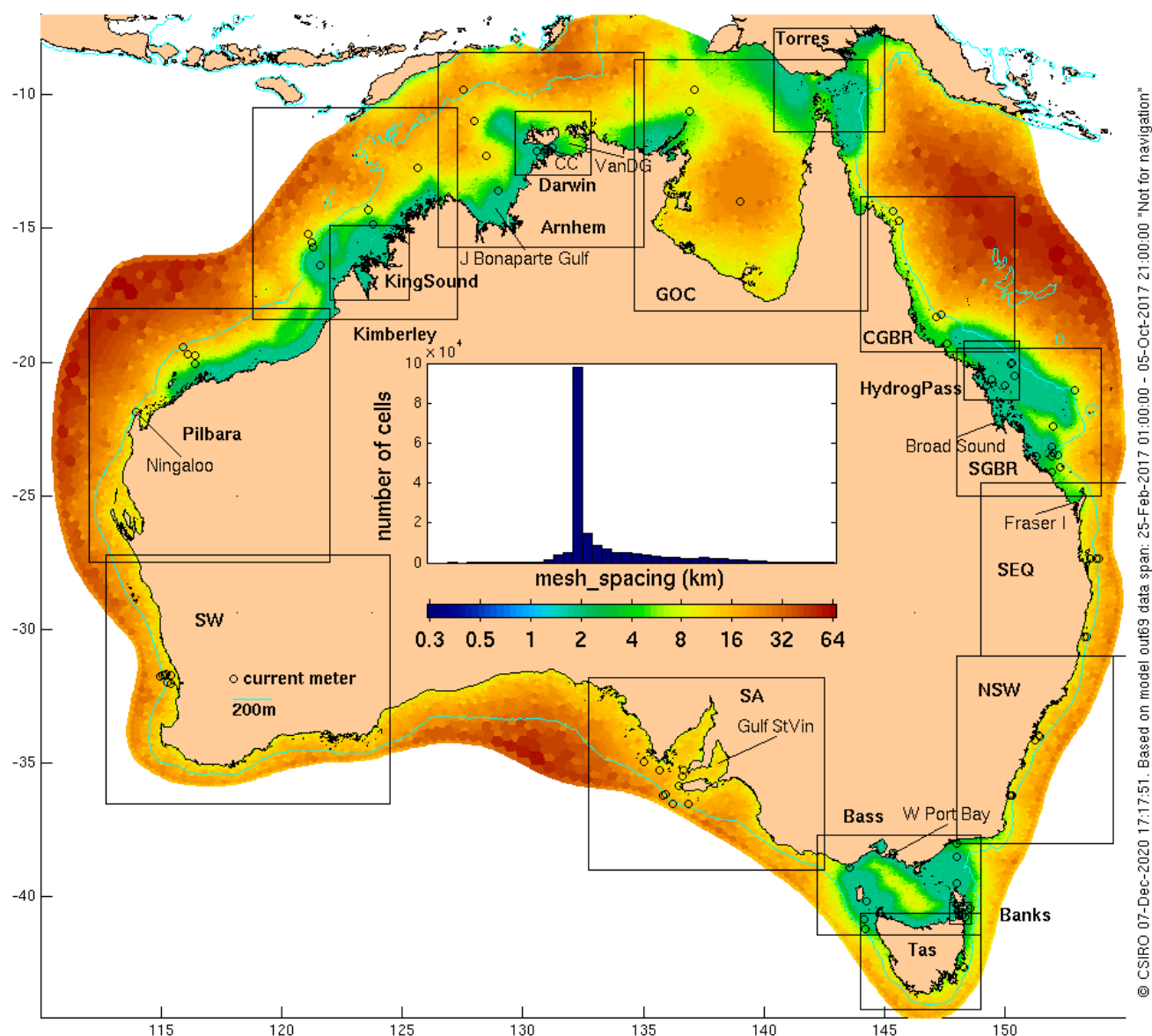
Figure 1 Model mesh spacing (km, log scale). Abbreviated names are: CC=Clarence Channel, VanDG=Van Diemen Gulf, GOC=Gulf of Carpentaria, CGBR=Central Great Barrier Reef, SGBR=Southern GBR, SEQ=Southeast Queensland, NSW=New South Wales, Bass=Bass Strait, Tas=Tasmania, Banks=Banks Strait, SA=South Australia, SW=South West.

2 Model configuration

We generated time-series of tidal predictions surrounding Australia using the unstructured model COMPAS (Coastal Ocean Model Prediction Across Scales) (Herzfeld et al., 2020). This model was chosen over structured model counterparts due to its capacity for superior resolution placement and transition, allowing high resolution to be exactly prescribed in areas of interest, and low resolution elsewhere. This significantly reduces the number of cells required to model such a large domain, resulting in an acceptable computational cost. COMPAS is a coastal ocean model designed to be used at scales ranging from estuaries to regional ocean domains. It is a three-dimensional (3D) finite volume hydrodynamic model based on the 3D equations of momentum, continuity and conservation of heat and salt, employing the hydrostatic and Boussinesq approximations. The equations of motion are discretised on arbitrary polygonal meshes according to the TRiSK numerics (Thuburn et al., 2009; Ringler et al., 2010), which is a generalisation of the standard Arakawa C-grid scheme to unstructured meshes. The horizontal terms in the governing equations (momentum advection, horizontal mixing and Coriolis) are discretised using the TRiSK numerics, whereas the pressure gradient and vertical mixing are discretised using the finite difference approach outlined by Herzfeld (2006). The horizontal mesh must be an orthogonal, centroidal and well-centred "primal-dual" tessellation, typically consisting of collections of Voronoi cells and their dual Delaunay triangles. The 3D model may operate using "z" or s vertical coordinates; however, in the present application a depth-averaged configuration is used. The bottom topography is represented using partial cells. COMPAS has a nonlinear free surface and uses mode splitting to separate the two-dimensional (2D) mode from the 3D mode. The model uses explicit time-stepping throughout, except for the vertical diffusion scheme which is implicit.

COMPAS uses the unstructured meshing library JIGSAW (Engwirda, 2017) to generate the underlying unstructured mesh. JIGSAW produces high quality meshes that support the requirements of the TRiSK numerics. The mesh of the model discussed here was generated using a dual weighting function dependent on bottom depth and tidal current speed, such that those regions with shallow water and high tidal velocities receive high resolution and vice versa. An initial configuration with resolution depending on tidal height amplitude gave poor results because some straits with strong flows but only moderate height amplitude received only moderate resolution. The mesh has 183,810 2D cells with an indicative cell size ranging from 332 m to 63 km (Fig. 1). Eighty per cent of cells have sizes between 1900 m and 7100 m. The mean length of edges in the mesh is 3680 m. Note that a regular structured grid covering the same spatial domain at the same mean resolution would require ~1.5 million 2D cells.

The model topography (Fig. 2) uses bathymetry from the Geosciences Australia (2002) database, with regions outside its extent filled using the global database dbdb2 (Naval Research Laboratory Digital Bathymetry Data Base https://www7320.nrlssc.navy.mil/DBDB2_WWW/). This was supplemented with high resolution datasets in the Great Barrier

Ocean Science
Discussions

Reef (Beaman, 2010) and northern Australia (https://ecat.ga.gov.au/geonetwork/srv/eng/catalog.search#/metadata/121620). Onsite depth measurements at the locations (Fig. 2) of the tidal currents validation data discussed below were not used for estimating the model topography. The minimum depth (at zero tide) in the model is 4 m for most of the grid, but 8 m in the NW, NE and in Gulf St Vincent. Depth was median filtered to remove sharp gradients. A deeper channel of 12 m was also

75   included in King Sound (in the NW). These bathymetric changes had significant effect on the tidal response, and it is anticipated that further model improvement will require targeted bathymetry modification at the local scale.
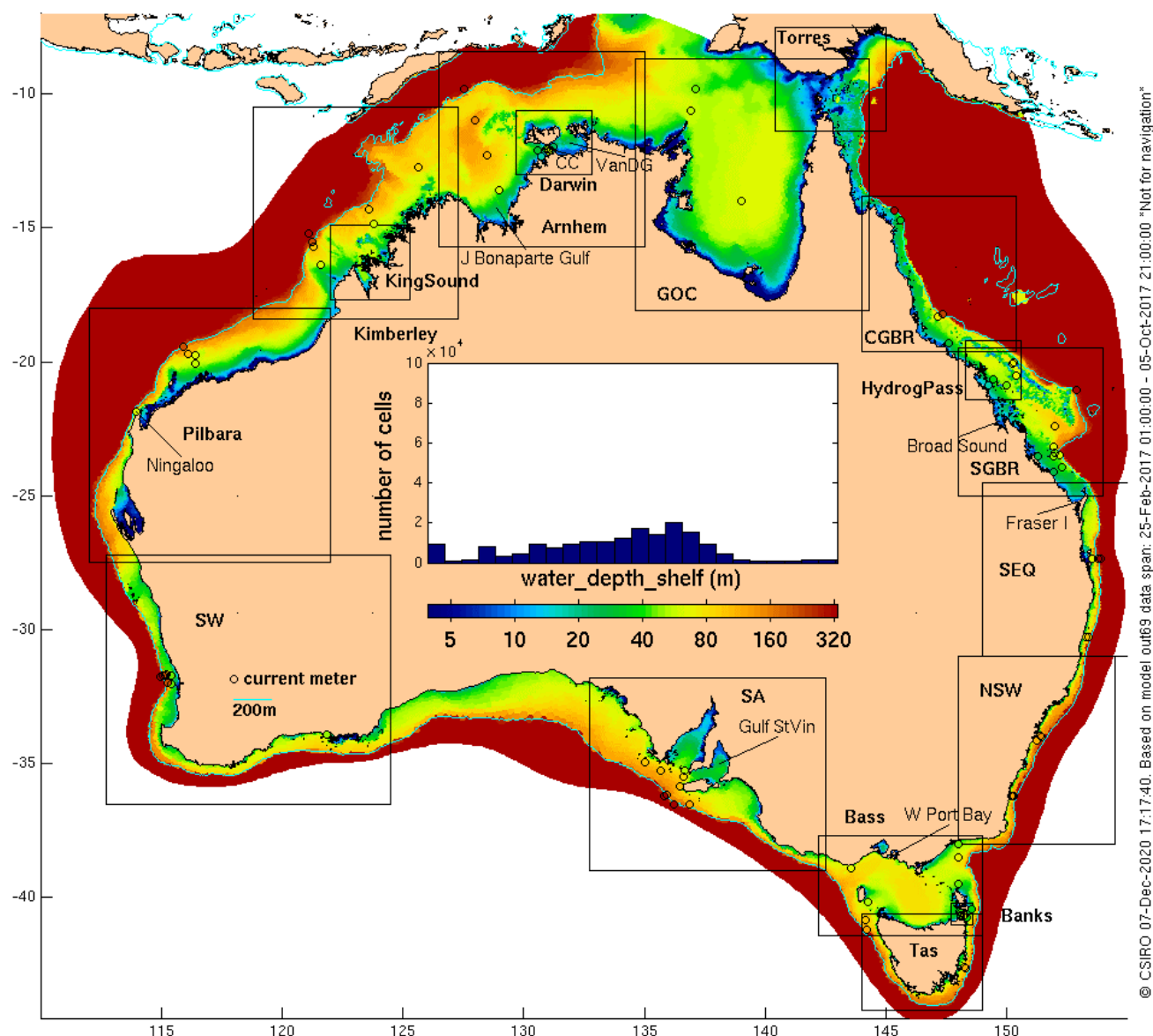

Figure 2 Model depth (m, log scale, spanning just a restricted range). Otherwise like Fig. 1.

The tide is introduced through eight tidal constituents (M2 S2 N2 K2 K1 O1 P1 Q1) from the TPXO9v1 1/6° global model
(Egbert and Erofeeva, 2002; http://volkov.oce.orst.edu/tides/otps.html) and applied at the open boundary using the condition
described by Herzfeld et al. (2020). The Herzfeld et al. (2020) scheme includes a normal and tangential velocity Dirichlet
condition with provision for a local flux adjustment on normal velocity to maintain domain-wide volume continuity. Thus, the
surface height is not directly constrained at the boundary but is instead computed via volume flux divergence as it is in the
model interior. For the present application, we found that flux adjustments to constrain the sea surface height were not required;
prescribing the transports at the boundary was sufficient to achieve the target height. This situation is quite unusual. One
necessary step to achieve this was to use the TPXO components of transport on their native (Arakawa C) grid and use the
depths in COMPAS to convert the transports to depth-averaged, cell-edge normal velocity, thus accounting for bathymetry
differences between our model and the TPXO model. The model was run in 2D mode only, using a time-step of 1 s, achieving
a runtime of ~5:1 on twelve processors. A spatially constant bottom drag coefficient of 0.003 was used to compute bottom
stress. Tidal potential forcing is optionally applied in the model but we found that it made very little difference compared with
other parameters such as friction, so we have omitted it for the configuration described here.

For many test runs of the model, it was started from rest and run for either 7 or 30 days from 24 Feb 2017 including a 1-day
ramp period. Results were compared with harmonically synthesised time series at all sites for which tidal constituents are
available (see below) using T-Tide (v1.3b, Pawlowicz et al., 2002) and then parameters were manually adjusted, or model
code de-bugged or improved, in search of closer agreement with the observations. Apart from this 'tuning', no data assimilation
was used with these model runs.

For the model configuration described here, it was run for 222 days from 24 Feb to 5 Oct 2017, and then tidally analysed so
that 1) its performance can be described for individual constituents, and 2) predictions can be made for any time or place within
the domain without having to run the model. The COMPAS model code, the output time series and tidal constituents at all
points of the mesh are freely available, as described in Sections 9 and 10.

3 Current meter observations

Acoustic Doppler current profilers (ADCPs) of various types have been deployed as part of Australia's Integrated Marine
Observing System (IMOS) at 55 sites over the continental shelf around Australia, some for several years, since 2007. The
ADCPs are almost all moored within a few metres of the sea bed, and sense the water velocity over the lower 80–85% of the
water column. We have taken the depth-average of these observations, concatenated all records from individual instrument
deployments at the same nominal position, and determined the tidal constituents using the UTide software of Codiga (2011).
Apart from the deployments off the NW of the continent, these sites tend to be at locations where tidal currents are not
particularly strong. As a means of quantifying the relative magnitude of tidal and sub-tidal depth-average velocity, we
determined the principal axis of the subtidal variability (using singular value decomposition) and computed the root mean
square (RMS) of the major and minor axis components. Details of the IMOS ADCP deployments are at

Ocean Science
Discussions

EGU

Open Access

http://oceancurrent.imos.org.au/timeseries/ along with regional graphics comparing the tidal and sub-tidal ellipse parameters (as well as the mean velocity for each deployment).

Penesis et al. (2020) give details of ADCP deployments that deliberately sought to observe tidal currents for two of Australia's most prospective tidal energy development regions. These include seven locations in the Clarence Channel near Darwin and

115   seven locations in Banks Strait at the NE tip of Tasmania. We determined tidal velocity constituents, the mean and sub-tidal ellipse parameters from these data as above.

We have included data from 10 of the sites where Middleton et al. (1984) and Griffin et al. (1987) deployed current meters on the Southern Great Barrier Reef (SGBR, see Fig. 2) in order to study both the anomalous tides and the sub-tidal variability. These observations were made by single, mechanical RCM4 Aanderaa current meters with several drawbacks compared to

120   ADCPs. Due to limited storage capacity, the flow direction was only sampled instantaneously once an hour, so short-period changes of direction were not averaged. To minimise noise due to waves, the instruments were moored fairly low in the water column (typically 7 m off the seabed), thereby probably underestimating the depth-average velocity. Some had to be deployed close to islands, with the result that they recorded effects (such as asymmetric ebb and flood directions) that the model is unlikely to be able to reproduce at specific locations due to its imperfect representation of topography. Nevertheless, we have

125   included these records in our validation dataset, processed as above, despite the quality questions because 1) the tides in this region are important for navigation (e.g. through Hydrographers Passage), and 2) in the hope that future models with finer meshes and better topography may be able to better distinguish observation error from model error.

Lastly, we also extracted 13 current meter records from the CSIRO archives (https://www.cmar.csiro.au/data/trawler/), choosing sites in Bass Strait, the NW shelf and the Gulf of Carpentaria where tidal currents are significant. These were mostly

130   point measurements, either by acoustic or mechanical (Aanderaa) current meters. Where two instruments were deployed on a mooring, we simply averaged the data for the period when both were operating.

In support of this paper and future studies of the tides of Australia, we have published this validation data set as a netCDF file containing up to 13 tidal constituents, and the subtidal statistics, for each of the 95 locations discussed above (see Section 10).

4 Tide gauges

135   The National Operations Centre (NOC) Tidal Unit of the Bureau of Meteorology (http://www.bom.gov.au/oceanography/projects/ntc/ntc.shtml) kindly provided tidal height constituents for 683 sites, of which 626 are within the COMPAS domain. To this we have added nine sites from the UNSW SGBR dataset bringing the total to 635 before applying quality control.

5 Model-data comparison method

140 All model-data comparisons presented in this paper are based on the six major tidal constituents (M2, S2, N2, K1, O1 and P1) determined from the model and observational time-series (rather than the time series approach used during model tuning) for all the usual reasons. The length of the analysed model run (222days) is long enough to resolve P1 from K1 but we do not discuss results for these lesser constituents (important as they are for predictions) in detail because the results for M2 are broadly representative of all constituents. Availability of the full set of model-data comparisons for 6 constituents, 18 regions

145 and 5 variables is covered in Section 10.

5.1 Tide gauges

When comparing the model with tide gauges, we select the closest model grid point if one exists within 11 km. We calculate the model error (model minus observation) for amplitude and phase individually as well as the vector error (taking both phase and amplitude into account) for each tidal constituent. Summing over a number of sites within a certain geographic region,

150 we then compute the Mean of the Absolute value of the amplitude Error (MAE), the Mean Magnitude of Vector Error (MMVE), the mean of the amplitude error and the mean of the observed amplitude (for expressing the MAE or MMVE as a relative error or RE). We use MAE and MMVE in preference to root-mean-squared errors because the MAE and MMVE are less affected by outliers. Outliers are a significant issue, as we will discuss below with reference to Table 1, which lists the sites we have chosen to exclude from the tidal heights dataset. We combine analyses for the six constituents by computing the

155 Root Sum of Squared (RSS) MAEs and MMVEs. In order to estimate the total regional-mean tidal relative error, we also compute the RSS of the area-mean observed amplitudes. These statistics are computed for a number of regions (bounding boxes are shown in Fig. 1) around Australia as well as for the entire country and listed in Table 2. We have not attempted to account for the uneven distribution of the data points around Australia, other than to compute regional means as well as the nationwide means. Nor have we attempted to estimate errors of the observational tidal constituents based on factors such as

160 record length or instrument type.

5.2 Current meters

When comparing with current meters, we select the grid point for which a penalty function J=D/(5C)+|H_m-H_o|/H_o is minimised, where D are the distances to the model grid point, C are the sizes of the cells, H_m are the model depths and H_o is the onsite depth at the observation point. This is an attempt to mitigate the effect of the model's imperfect topography, by

165 finding the nearest depth-matching (if possible) model counterpart of the observation. We then proceed as for tide gauges, but with the amplitude and phase of the major axis velocity taking the place of height. Errors of the major axis inclination and minor axis amplitude are shown graphically and are listed in Table 3 but are not otherwise included. Three sorts of site-specific relative error are listed in Table 3: 1) the M2 major axis velocity amplitude error relative to the observed amplitude $reM2 = (|maj_m| - |maj_o|)/|maj_o|$, 2) the M2 major axis velocity vector error relative to the observed amplitude $re\overline{M2} =$

7

Ocean Science
Discussions

Open Access

EGU

170 $|maj_m - maj_o|/|maj_o|$, and 3) reLF, which has the observed sub-tidal ('low frequency') RMS major axis velocity sub_o included in both numerator and denominator. The first two measures characterise the model's ability to do what it is designed for, which is just to simulate tides. The first of these is for users who need to know tidal range but not at any particular time. The second is for applications where timing is also important. The third acknowledges that tides are not the dominant component of velocity variability everywhere. Using a tidal model alone (i.e. without a model of other processes) to predict

175 the total current (characterised by maj_o+sub_o) will result in an error determined by sub_o if the tidal error is zero. Where tidal and sub-tidal variability are equal, the upper limit of reLF is 50%.

Table 3 lists sites by ascending reLF, and includes averages of the sites with lowest, middle and greatest reLF, for most columns. For the '*m-o*' column the average is mathematically an MAE, but with a non-geographic sample of sites. Table 4 is like Table 2, with major axis velocity amplitude and phase taking the place of height amplitude and phase, for the same six

180 constituents.

6 Results

6.1 Tidal height

Since we have no reliable, objective (model independent) way of knowing which tide gauge observations (or more precisely, the analysed tidal constituents) are more accurate than others, we have cautiously employed a largely model-based quality

185 control procedure. This procedure excludes sites if:

- The absolute value of M2 error exceeds 20 cm and an observed M2 amplitude within 10 km is less by more than 20 cm (excludes four sites)

- The observed amplitude is less than 4 cm (two sites)

- The observed amplitude exceeds 10 cm and is less than half, or more than twice the model amplitude (14 sites)

190 - The observed and modelled phase differ by more than 90° (six sites).

Table 1: Blacklisted tide gauges. Tests are on the nearest neighbour difference (cm), the observed M2 amplitude and the model M2 amplitude and phase relative to the observed values.

Site#	Site	Latitude	Longitude	nndiff	Observed	Model	Phase diff
67	Kai-Maituine Reef - Northeast	10.23S	143.15E	0	69	60	100
105	Sharp Point	10.97S	142.72E	-49	23	91	-32
125	Harvey Island	11.97S	143.27E	-44	19	74	6
152	Endeavour River North	15.43S	145.2E	-22	31	57	-3
187	Rib Reef	18.47S	146.87E	0	22	68	-3
333	South Channel	38.3S	144.71E	-5	21	9	31
378	Maatsuyker Island	43.67S	146.32E	0	23	9	25

457	Nornalup Inlet	35S	116.73E	0	2	6	-48
465	Mandurah	32.53S	115.72E	0	3	5	-13
490	Monkey Mia	25.8S	113.72E	0	38	9	28
577	Bonaparte Gulf	12.83S	128.47E	0	14	82	-132
586	Catfish Island	14S	129.48E	86	268	173	-42
631	Peacock Island	11.02S	132.45E	0	19	64	21
659	Mallison Island	12.18S	136.1E	0	173	12	94
668	Centre Island	15.75S	136.81E	0	40	15	47
669	Mornington Island	16.67S	139.17E	0	14	7	44
670	West Wellesley Islands	16.8S	138.96E	0	16	8	41
672	Albert River Mouth	17.55S	139.76E	0	20	10	125
674	Sweers Island	17.11S	139.59E	0	15	5	115
675	Karumba	17.49S	140.83E	0	17	14	97
	Failure criterion			>20cm	<4cm	o*0.5, o*2	>90 °
	Number of failures			4	2	14	6

195

With the 20 sites listed in Table 1 excluded, the M2 MAE across 615 sites is 9.3 cm, or 13 % of the mean observed amplitude, which is 72.5 cm. The resulting scatter plot (Fig. 3, note the log-log axes) of model vs observed height amplitude still has points that could be considered outliers; at 5 % of sites the negative errors are ~3 to 10 times the MAE. But we have not excluded these along with the other 20, for lack of clear evidence that they are due to observation error rather than model error.

200 The bias is relatively small but not insignificant (-2.3 cm, see Table 2). It is negative because most of the biggest errors are cases of the observation exceeding the modelled amplitude. The region with the biggest negative M2 bias (-11 cm) is clearly (see Table 2) the Southern Great Barrier Reef, where the model underpredicts the large tides within about 100 km of the head of Broad Sound

The region with the biggest M2 amplitude MAE is the one we abbreviate here as 'Arnhem' (rather than Joseph Bonaparte Gulf

205 and Arnhem Land) but across this region there is a mix of under and over-prediction. The modelled M2 height amplitude is too small in Van Diemen Gulf and the head of Joseph Bonaparte Gulf but too great at many of the offshore sites where the observed amplitude is small.

There are large M2 phase errors (Fig. 4) at many sites. While some are possibly due to observation error, the predominance of positive phase errors, especially in regions of strong tides, points to a problem in the model. The region with the biggest M2

210 phase MAE is the Kimberley (20°) (Table 2), nearly twice the all-site average of 11.5°. The significant phase errors are why the Australia-wide M2 MMVE (20 cm) is so much greater than the M2 MAE (9.3 cm).

The next most energetic constituent after M2 (72.5 cm averaged across all sites) is S2 (35.8 cm). S2 has the next-greatest MMVE (12.9 cm, because of large phase errors in the Kimberley), then K1 (with 29.6 cm observed amplitude) has a MMVE of 7.7cm.

215 Summing over six constituents, and taking both phase and amplitude errors into account, the RSS MMVE across all sites is 26.1 cm, or 29.1 % of the mean observed amplitude. The three regions with the lowest relative error (11.9, 14.4 and 16.8 %)

are Central Great Barrier Reef, New South Wales and the South West, while the three regions with the highest (38.9, 36.4 and 35.6%) are the wide shallow seas in the tropics: Torres Strait, Joseph Bonaparte Gulf and Arnhem Land and Gulf of Carpentaria. Thus, the greatest regional-average relative errors of modelled height are about twice the size of the least. Both

220   are small enough to conclude that the model has skill, but large enough to conclude that there is still room for improvement.
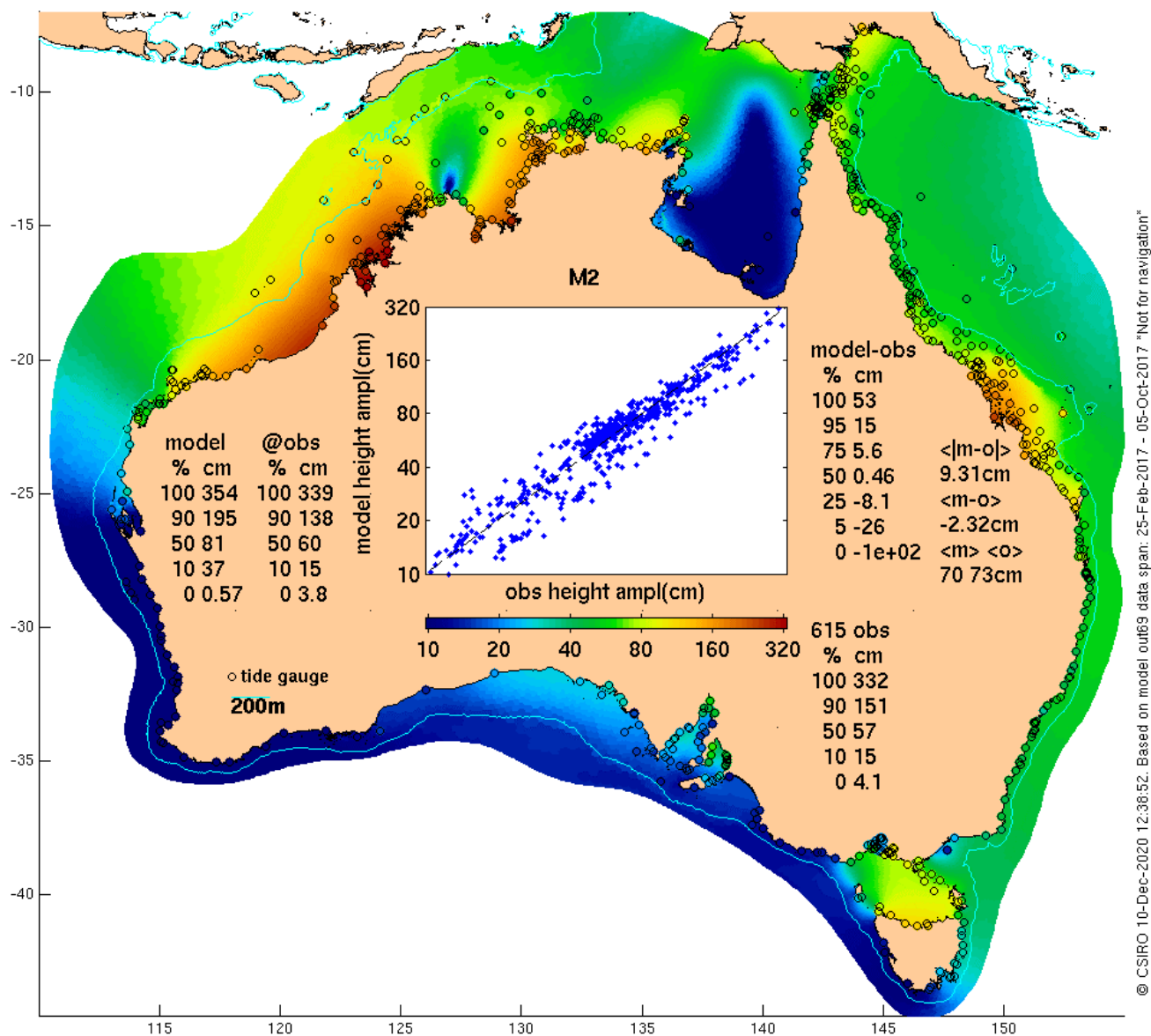
Figure 3 M2 height amplitude as a colour-fill map (the model) and points (observations), and inset as a quantity-quantity plot. Statistics listed are percentiles of 1) the whole model height field, 2) m=model at validation sites, 3) model error m-o and 4) o=observed values. <|m-o|> is the Mean of the Absolute value of m-o. <m-o> is the mean error, or bias. <m> and <o> are the mean modelled and observed amplitudes. A log scale is used, starting at 10cm, so not all points can be shown.
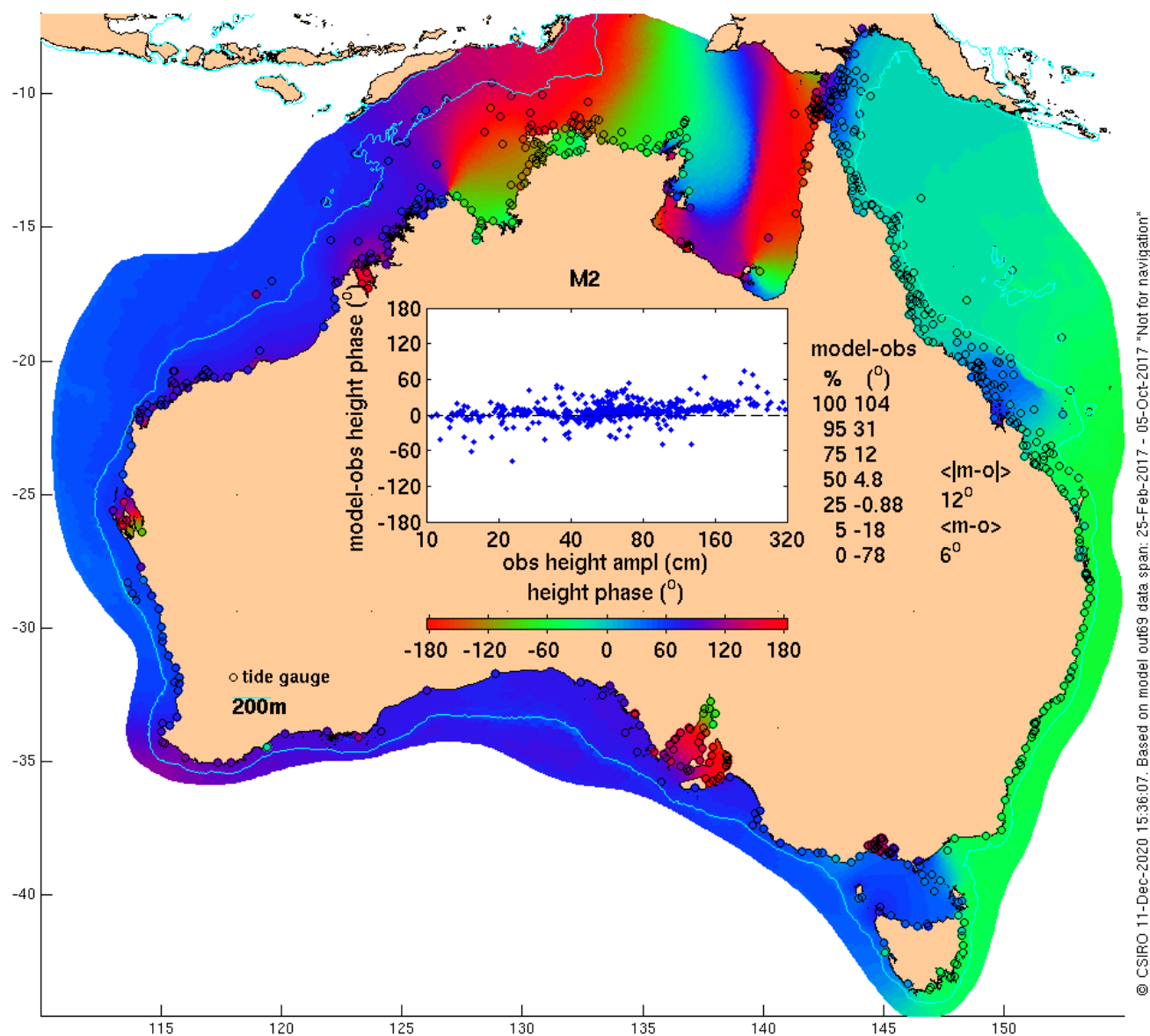
230 **Figure 4 M2 height phase (otherwise like Fig. 3, except the y-axis of the inset is the phase error rather than phase).**

235

Table 2: Tidal height and phase region-average statistics, for 6 constituents (and their root sum of squares).
Height (cm)
mean observed amplitude < o >

	Aust	Arnhem	GOC	Torres	CGBR	SGBR	SEQ	NSW	Bass	Tas	SA	SW	Pilbara	Kimb.
#sites	615	78	111	67	59	67	29	27	54	24	62	31	41	43
M2	72.5	112.1	59.2	60	56.5	112.4	59.7	46.5	56.7	46.5	25.5	6.6	77.5	168.3
S2	35.8	50.1	34.7	41.1	33	42.2	17.5	11.1	12.1	7	26.7	7	44.4	99.5
N2	16	21.7	18.3	20.8	18.6	27.7	11.8	10.5	11.8	9.3	1.9	2.1	11.8	26.5
K1	29.6	42.2	42	47.2	31.4	31.9	18.9	15	15.9	17.3	24.2	17.5	21.2	31.6
O1	17.6	27.1	24.3	23.9	15.1	16.4	10.6	9.4	10.9	12	16.5	12.6	13.6	19.3
P1	8.5	11.7	12.2	13.7	9.4	9.6	5.1	4.5	4.8	4.2	7	5.4	5.9	8.7
RSS	89.7	134.9	86.9	93.3	77	128.6	67.2	52.2	62.4	52.5	47.6	24.4	93.7	200.9

240 **mean magnitude of vector error (MMVE)**

	Aust	Arnhem	GOC	Torres	CGBR	SGBR	SEQ	NSW	Bass	Tas	SA	SW	Pilbara	Kimb.
#sites	615	78	111	67	59	67	29	27	54	24	62	31	41	43
M2	20	36.4	20.2	20.6	7	23.3	17.1	6.2	12.8	7.9	9.6	1.7	23.5	55.9
S2	12.9	22.6	14.3	19.3	4.6	9.5	7	2.4	3.4	2.9	11.2	1.1	17.3	42.1
N2	5.1	7.4	6.7	8	3	7.3	3.8	1.7	3.5	3.6	0.92	0.6	5.2	11.5
K1	7.7	19.1	14	17.7	2.1	3.3	3.9	2.5	3	3.8	5.6	2.6	5.3	7
O1	4.6	11.3	8.9	10.2	1	1.9	2.2	1.5	1.9	2.3	3.4	2	3.1	4.2
P1	2.5	5.2	4.8	6.1	0.84	1.1	1.7	0.87	1.1	2.4	1.7	1.1	2	2.2
RSS	26.1	49	30.9	36.2	9.2	26.5	19.4	7.5	14.2	10.5	16.3	4.1	30.3	71.4
%obs	29.1	36.4	35.6	38.9	11.9	20.6	28.9	14.4	22.8	19.9	34.2	16.8	32.4	35.5

mean absolute value of error <|m-o|> (MAE)

	Aust	Arnhem	GOC	Torres	CGBR	SGBR	SEQ	NSW	Bass	Tas	SA	SW	Pilbara	Kimb.
#sites	615	78	111	67	59	67	29	27	54	24	62	31	41	43
M2	9.3	17.7	10.9	8.9	5.4	12.4	6.2	4.8	8	3.4	7.2	0.78	6.1	12.6
S2	5.7	10.2	8.3	11	2.4	4.8	3.5	2.2	2.1	1.3	7.9	0.6	4.3	7.9
N2	3	4.4	3.9	4.3	1.9	4.7	2	1.2	2.5	2.4	0.53	0.42	2.9	4.7
K1	3.5	4.7	8.1	9.3	1.6	1.5	1.6	1.9	2.3	2.1	3.2	1.2	2.1	2.7
O1	1.9	2.6	3.7	3.2	0.75	1.2	0.75	0.91	1.4	1.4	1.7	0.88	1.3	1.8
P1	1.3	1.7	2.6	3	0.62	0.54	0.97	0.67	0.86	2.1	0.97	0.5	1.1	1.2
RSS	12	21.6	17	18	6.4	14.2	7.7	5.8	9	5.5	11.3	1.9	8.5	16
%obs	13.4	16	19.6	19.3	8.4	11	11.4	11.1	14.5	10.4	23.8	7.8	9.1	8

mean error < m-o > (bias)

	Aust	Arnhem	GOC	Torres	CGBR	SGBR	SEQ	NSW	Bass	Tas	SA	SW	Pilbara	Kimb.
#sites	615	78	111	67	59	67	29	27	54	24	62	31	41	43
M2	-2.3	-5.2	-2.2	-0.45	4.9	-11	4.9	4.2	-5.2	-0.95	-2.6	-0.49	2.2	-5
S2	-0.93	0.85	-6.3	-10	1.8	-3.4	3.2	2.1	-0.98	-0.4	0.97	-0.29	2.2	-0.74
N2	-1.2	-2.8	-2.7	-3.7	0.48	-4.1	1.6	0.88	-1.1	1.4	0.32	-0.23	1.7	-1.7
K1	-1.3	-0.85	-6.7	-8.6	0.29	-0.75	1.3	1.6	0.75	0.57	-2.2	0.025	0.75	0.064
O1	-0.54	-0.15	-2.4	-1.8	0.25	-1.1	0.37	0.68	0.49	0.2	-1.1	0.038	0.43	-0.19

12

Ocean Science
Discussions

EGU

	Aust	Arnhem	GOC	Torres	CGBR	SGBR	SEQ	NSW	Bass	Tas	SA	SW	Pilbara	Kimb.
P1	-0.32	-0.38	-2.1	-2.8	-0.11	-0.37	0.91	0.55	0.33	1.3	-0.6	0.16	0.48	0.53

245

Height phase (°)
mean absolute value of error <|m-o|> (MAE)

	Aust	Arnhem	GOC	Torres	CGBR	SGBR	SEQ	NSW	Bass	Tas	SA	SW	Pilbara	Kimb.
#sites	615	78	111	67	59	67	29	27	54	24	62	31	41	43
M2	11.5	13.7	15.6	16.4	3.7	8.2	12.9	3.8	9.4	9.1	12.8	9.3	15.1	20.3
S2	14.5	18.7	20.1	25.8	5.8	9.4	15	4.6	11.9	21	15.1	5.1	18.8	25.3
N2	14.3	15.1	18.2	19.3	5.5	9.4	14.1	5.4	13.3	19.1	17.1	11.3	18.9	25.2
K1	10.4	23.9	14.2	18.3	2.1	4.6	9.4	5.2	5.7	9.7	9.7	7	11.1	10.5
O1	10.6	23	17.1	22.9	1.7	4.1	10.5	6.7	4.9	7.6	9.2	7.9	9.7	10.4
P1	13.4	22.8	17.5	21.5	2.9	4.9	11.7	5.5	9.6	26.4	10.3	9.4	23.8	16.9

mean error < m-o > (bias)

	Aust	Arnhem	GOC	Torres	CGBR	SGBR	SEQ	NSW	Bass	Tas	SA	SW	Pilbara	Kimb.
#sites	615	78	111	67	59	67	29	27	54	24	62	31	41	43
M2	5.9	11.1	11.9	13.7	2.2	6.5	-7.9	-3	5.4	5.2	-2.5	0.43	10.7	16
S2	7.1	13	11.5	12.1	5.4	7.5	-7.4	-3.6	6	1.3	-0.39	-1.1	15.6	19.7
N2	6.3	10.6	11.8	14.8	1.4	7	-9.3	-2	5.1	-3	1.9	0.95	12.7	19.8
K1	6.2	23.4	9.4	17.3	-0.44	4.3	-5.7	-3.3	1.2	0.94	3.2	3.1	7.7	7.9
O1	7	22.7	15.4	22.8	0.55	3.2	-7.3	-4.7	0.15	1.5	3.3	3.6	6.8	8.2
P1	3.7	21.7	11	20.5	-1.4	3.9	-6.5	-4.4	-2.4	-19	4	0.9	-4.3	-2.4

250

Figure 5 Amplitude of the M2 major axis velocity, otherwise like Fig. 3. Black (model, at a random subset of grid points) and magenta (observed) velocity ellipses use the scale shown.

6.2 Tidal currents

Perhaps the most striking difference between maps of the M2 major axis amplitude (Fig. 5) and the M2 height amplitude (Fig. 3) is that the currents have more small-scale variability, clearly associated with the local topography, as well as the regional variability that broadly reflects the regional variations of tidal range. Characterising and analysing the distribution of the errors

260   as well as the signal is not straightforward, but is what we will attempt to do, after looking at some of the site-specific results listed in Table 3.

The first line of Table 3 is for a Gulf of Carpentaria site sampled in 1987 by CSIRO. It is the first line because it has the lowest reLF, which in turn is because the errors of the M2 major axis velocity phase and amplitude are both small (0° and 1 cm s^{-1}), while the amplitude of the observed M2 tidal currents is large (21 cm s^{-1}) compared to the rms sub-tidal velocity (3 cm s^{-1}).

265   Site CW3 (line 2) sampled by Penesis et al. (2020) in Banks Strait is a much more energetic site but the errors of the major axis velocity phase and amplitude are both relatively small (8° and 1 cm s^{-1}) nevertheless. It is also a tidally dominated site, (98 cm s^{-1} for M2 compared to the sub-tidal velocity of just 7 cm s^{-1}). As it happens, the error of the minor axis is also very small (both are essentially zero) here, but the error of the inclination is not (-28°T observed but -52°T modelled). Site CW1 (line 3) is about 3 km away (just one grid cell) and has a greater amplitude error (13 cm s^{-1}) but less inclination error (3°).

270   Looking down the table we see that 9 of the 19 lowest-error sites are in Banks Strait. This is clearly a region where the model in its present form is capable of producing current velocity predictions with low relative error (reM2, re$\overline{M2}$ and reLF 17, 26 and 30 % at most), so is the first to be discussed in the next section.

At the other extreme (at the bottom of Table 3) is NRSNIN, an IMOS ADCP at the Ningaloo Reef National Reference Site in Western Australia, where the observed M2 major axis amplitude is just 7 cm s^{-1}. The model estimate is listed as being more

275   than twice this, at 19 cm s^{-1}. From the prediction point of view, these errors are compounded by there being a fairly large (18 cm s^{-1}) sub-tidal variance at this site. Similarly, the next-highest relative error is at GBRLSL, a site off the Great Barrier Reef in 330 m of water where the observed M2 major axis velocity is essentially zero, but the model estimate is 7 cm s^{-1}. One thing these two sites have in common is that they are over steep topography where sharp gradients are common, so part of the poor agreement is bound to be due to representation error (that error that occurs when you compare a point measurement with

280   an area-average). But even so, these are probably not sites where tidal predictions will be of much practical use.

Table 3 includes statistics that characterise model error averaged over sites grouped according to whether reLF is in the lowest, middle and highest third. The MAE over this first third is 7 cm s^{-1} (an 11 % average relative error), while the MMVE is 13 cm s^{-1}, a 22 % average relative error or 29 % if sub-tidal currents are taken into account as well. For the locations that these sites are representative of, you could argue that the tidal model is not only useful, but is enough by itself, i.e. a short-term forecast

285   of sub-tidal current velocity would not often make a significant contribution (since its rms value is around 6 cm s^{-1}, just 10% of the average M2 amplitude). For the middle group the average M2 tidal current amplitude (30 cm s^{-1}) alone still exceeds the sub-tidal variability (9 cm s^{-1}), but the dominance is less than for the first third and the errors of the tidal model are not insignificant. The average reLF for this group is 57 %, which could be argued as being acceptable, but with there being much room for reduction, either by improvements to the tidal model or addition in near-real time of a skilful forecast of sub-tidal

290   variability. For the final third, the observed tidal currents are mostly insignificant (3 cm s^{-1} compared to 22 cm s^{-1}), so it doesn't really matter what the predicted tidal velocity is, as long as it is weak. This last group includes all 11 sites in New South Wales and south-east Queensland regions, five of the deeper (~100 m or more) sites in South Australia, and all eight of the sites in

south-west Western Australia. We will now look more closely at the regions where tidal currents are a large fraction of the variability.

295

Table 3: Model errors for the M2 constituent at current meter sites. Columns: h_o and h_m are observed and modelled depth, |mean| and dir are the magnitude and direction of the mean observed velocity while sub_o is the rms observed sub-tidal velocity along its major axis. The modelled and observed major axis amplitudes are maj_m and maj_o (or m and o for short) so m-o is the amplitude error and normalising by o gives the relative error reM2. Taking phase into account we have |m̃-õ|, the magnitude of the vector error and the relative vector error $\overline{reM2}$ = |m̃-õ|/o. Including rms sub-tidal variability sub_o we have reLF=(|m̃-õ|+sub_o)/(o +sub_o). Sites are ordered by reLF. Averages over thirds and all of the sites are given.

300

Row	Site	Region	lat.	long.	h_o	h_m	|mean|	dir	sub_o	inc_o	maj_o	min_o	inc_m	maj_m	min_m	m-o	m-o	|m̃-õ|	reM2	$\overline{reM2}$	reLF
			°S	°E	m	m	cm s⁻¹	°T	cm s⁻¹	°T	cm s⁻¹	cm s⁻¹	°T	cm s⁻¹	cm s⁻¹	°	cm s⁻¹	cm s⁻¹	%	%	%
1	ARA-GOC87	GOC	10.64	136.94	57	58	7	-42	3	-86	21	6	-79	22	1	0	1	1	6	6	17
2	CW3	Bass	40.55	148.08	33	31	4	115	7	-28	98	0	-52	98	1	8	1	14	1	14	20
3	CW1	Bass	40.53	148.06	32	30	0	90	0	-52	81	-2	-55	94	1	7	13	16	16	20	20
4	CW4A1	Bass	40.67	148.09	30	32	6	84	9	-71	133	-3	-70	128	-1	9	-6	21	4	16	21
5	ARA-GOC87	GOC	9.818	137.12	47	46	3	61	2	81	21	7	80	21	4	-8	0	3	1	14	22
6	GBRHIN	SGBR	23.38	151.99	45	41	3	-33	8	78	50	8	80	45	6	1	-5	5	10	10	22
7	CWTb1	Bass	40.68	148.23	63	45	16	128	9	-68	87	-3	-69	99	0	4	11	13	13	15	22
8	CW2A1	Bass	40.58	148.1	44	33	9	121	11	-50	123	-3	-54	123	0	9	0	20	0	16	23
9	ITFFTB	Arnhem	12.29	128.48	108	105	4	121	6	-52	35	-7	-54	37	-7	5	2	4	6	11	23
10	NRSDAR	Arnhem	12.34	130.71	18	16	3	79	4	-59	55	7	-60	60	8	9	5	10	9	19	24
11	BASS-CS91	Bass	40.14	144.25	53	50	3	42	10	46	58	7	47	53	7	5	-6	7	10	13	26
12	CW2A2	Bass	40.7	148.2	44	39	12	156	7	-38	85	-2	-60	95	0	9	10	18	12	21	27
13	C1A1	Bass	40.67	148.24	56	42	14	130	8	-75	84	-2	-76	97	0	7	13	17	16	20	28
14	GBRHIS	SGBR	23.51	151.96	47	45	2	40	4	88	32	2	83	37	5	5	5	6	15	18	28
15	CW4A2	Bass	40.73	148.34	36	36	7	87	5	-72	66	14	-75	70	11	12	3	15	5	22	28
16	DARBGF	Arnhem	12.11	130.59	30	30	1	-47	1	-89	56	6	-89	63	4	13	7	15	12	26	28
17	Darwin_C3	Arnhem	12.07	131.02	56	30	7	88	5	89	118	-2	79	96	0	11	-22	31	19	26	29
18	BASS-CS91	Bass	39.5	148.01	47	42	6	137	4	61	50	11	75	61	14	6	11	12	22	24	30
19	C1A3	Bass	40.69	148.12	27	25	12	12	8	-75	144	-1	-67	119	-1	12	-24	37	17	26	30
20	North Rf	SGBR	23.16	151.96	62	58	4	2	7	-75	44	4	-81	45	3	11	0	8	1	19	30
21	KIM100	Kimberley	15.68	121.3	99	96	5	213	11	-49	40	13	-53	39	13	7	0	5	0	12	31
22	KIM200	Kimberley	15.53	121.24	208	215	5	241	9	-59	22	7	-56	21	9	2	-1	1	3	5	32
23	KIM050	Kimberley	16.39	121.59	59	56	3	257	8	-72	44	26	-74	48	28	11	4	10	10	22	33
24	DarwinCTbW	Arnhem	12.02	130.97	22	22	9	234	2	65	89	-1	85	93	-1	21	3	34	4	38	39
25	CAM050	Kimberley	14.85	123.8	58	58	2	65	5	-35	64	7	-38	59	8	20	-5	22	8	34	39
26	GBRCCH	SGBR	22.41	151.99	93	87	6	123	7	-70	28	0	-67	32	-1	10	4	7	14	24	39

Ocean Science
Discussions
Open Access

Row	Site	Region	lat. $^\circ$S	long. $^\circ$E	h_o m	h_m m	|mean| cm s^{-1}	dir $^\circ$T	sub_o cm s^{-1}	inc_o $^\circ$T	maj_o cm s^{-1}	min_o cm s^{-1}	inc_m $^\circ$T	maj_m cm s^{-1}	min_m cm s^{-1}	m-o $^\circ$	m-o cm s^{-1}	|m̄-ō| cm s^{-1}	reM2 %	reM2̄ %	reLF %
27	Darwin_CW2	Arnhem	12.06	130.95	34	30	8	61	4	73	83	0	75	94	3	18	11	30	13	37	39
28	BASS-CS91	Bass	38.91	143.54	64	56	2	81	8	67	38	4	82	47	2	-7	10	11	25	29	41
29	C. Capricorn	SGBR	23.51	151.29	26	27	2	-56	9	-37	39	-7	-38	28	-5	2	-11	11	27	27	42
30	TIMORS88	Kimberley	12.76	125.66	91	92	2	23	4	47	23	-1	54	31	6	-2	8	8	33	33	43
31	GBROTE	SGBR	23.48	152.17	60	61	4	-22	17	70	29	10	74	31	2	-2	2	2	7	9	43
32	ITFJBG	Arnhem	13.61	128.97	61	56	1	226	4	-29	34	-10	-30	44	-18	11	10	12	28	36	43
mean abs. value	N=32				57	53			6		62			63		8	7	13	11	22	29
33	NW Shelf M6	Pilbara	19.74	116.39	65	64	3	112	6	-54	25	5	-43	32	3	6	7	8	27	30	43
34	CAM100	Kimberley	14.32	123.6	99	96	5	92	12	-37	47	9	-39	48	9	17	1	14	2	29	43
35	Darwin_CW3	Arnhem	11.95	131.23	22	20	9	98	3	46	76	7	49	87	2	21	11	32	14	41	44
36	CW6A1	Bass	40.43	148.54	37	33	16	35	9	22	36	7	27	26	8	-10	-10	11	27	31	45
37	Tas91UNSW	Bass	40.84	144.14	95	93	3	111	4	27	15	6	34	19	8	0	5	5	31	31	47
38	Round Hill Hd	SGBR	24.11	151.96	26	25	1	218	9	-75	16	0	-74	14	1	-4	-3	3	16	17	48
39	BASS-CS91	Bass	38.5	148	70	65	3	-58	11	72	24	8	69	29	10	3	6	6	24	24	48
40	BASS-UN91	Bass	41.18	144.23	115	116	5	151	6	42	14	8	33	11	4	-9	-3	4	22	26	49
41	SAM6IS	SA	35.5	136.6	83	85	3	188	8	57	9	0	55	9	1	-5	0	1	2	9	50
42	PIL050	Pilbara	20.05	116.42	55	52	2	268	12	-50	25	4	-48	30	1	6	6	6	22	25	50
43	CW6A2	Bass	40.43	148.53	31	33	4	94	6	46	45	4	27	26	8	7	-19	20	42	43	50
44	PIL100	Pilbara	19.69	116.11	105	114	7	223	13	-53	21	2	-51	24	1	5	3	4	16	19	50
45	PIL200	Pilbara	19.44	115.92	208	239	8	231	11	-73	13	0	-64	14	0	0	1	1	7	7	51
46	Darwin_CW1	Arnhem	12.1	131.12	22	21	7	199	4	-90	108	0	-85	53	5	11	-56	57	51	53	54
47	Darwin_C1	Arnhem	12.13	131.05	52	30	6	51	4	78	156	-1	89	80	2	18	-76	83	49	54	55
48	Wigton I	SGBR	20.67	149.47	38	39	6	66	9	-8	40	3	-1	42	5	25	3	18	6	46	56
49	NRSYON	CGBR	19.3	147.62	30	29	1	-30	18	-29	18	9	-30	16	11	5	-2	2	11	13	57
50	KIM400	Kimberley	15.22	121.11	396	371	1	-85	7	-64	10	5	-57	12	5	-6	3	3	27	30	59
51	ITFMHB	Arnhem	11	128	146	130	1	74	9	-34	14	-6	-36	19	-4	-8	5	5	35	39	63
52	BASS-CS91	Bass	38	148	47	45	1	137	10	72	12	2	66	15	2	-10	3	4	27	33	64
53	ARA-GOC87	GOC	13.99	139.03	60	62	2	-2	3	-54	7	4	-64	7	3	27	1	3	9	50	65
54	GBRPPS	CGBR	18.31	147.17	72	71	5	205	15	40	13	4	30	17	4	7	4	4	31	34	70
55	W Bugatti Rf	SGBR	20.08	150.25	70	51	13	178	3	33	55	4	12	93	19	9	38	39	68	71	73
56	Brampton I	SGBR	20.85	149.27	18	18	2	5	10	-9	32	-4	-3	41	3	32	8	21	26	66	74
57	NRSKAI	SA	35.83	136.45	103	110	12	192	20	17	8	0	14	8	1	-8	0	1	6	14	76
58	GBRLSH	CGBR	14.7	145.63	32	31	2	-84	15	15	13	2	71	9	0	-26	-4	6	29	48	76
59	N Bugatti Rf	SGBR	20.03	150.3	64	47	12	54	7	19	48	8	46	83	7	6	35	36	73	74	78
60	TASE88	Tas	42.65	148.28	110	104	9	5	13	-2	6	1	-2	4	0	-7	-2	2	30	31	79
61	SAM2CP	SA	35.28	135.67	100	99	5	-36	13	56	4	1	56	5	1	-8	1	1	12	19	80
62	NRSMAI	Tas	42.6	148.23	90	93	5	18	15	-4	6	1	-10	4	0	7	-2	2	32	34	82
63	SAM8SG	SA	35.25	136.69	53	47	2	92	10	41	9	3	28	14	2	-12	5	6	60	66	84

Row	Site	Region	lat.	long.	h_o	h_m	|mean|	dir	sub_o	inc_o	maj_o	min_o	inc_m	maj_m	min_m	m-o	m-o	|m̄-ō|	reM2	reM̄2	reLF
			$°S$	$°E$	m	m	$cm\,s^{-1}$	$°T$	$cm\,s^{-1}$	$°T$	$cm\,s^{-1}$	$cm\,s^{-1}$	$°T$	$cm\,s^{-1}$	$cm\,s^{-1}$	$°$	$cm\,s^{-1}$	$cm\,s^{-1}$	%	%	%
64	Creal Rf	SGBR	20.5	150.4	69	69	3	230	3	17	23	8	17	38	9	27	15	20	63	86	88
mean abs. value	**N=32**				81	78			9		30			29		11	10	13	35	45	58
65	SAM5CB	SA	34.93	135.01	98	95	2	104	23	15	3	1	14	3	1	1	1	1	27	27	93
66	GBRELR	SGBR	21.04	152.89	305	316	48	116	41	53	5	1	86	6	-1	11	1	2	27	35	93
67	SAM3MS	SA	36.15	135.9	168	160	18	142	21	55	3	2	33	3	1	-26	0	1	13	49	94
68	CH100	SEQ	30.26	153.4	97	92	31	199	37	-14	2	1	-72	2	1	13	0	1	6	25	96
69	BMP070	NSW	36.19	150.19	74	61	10	182	17	-21	1	0	-30	1	1	-20	0	0	18	41	96
70	CH070	SEQ	30.27	153.3	76	92	18	200	27	-17	2	1	-72	2	1	23	0	1	22	50	97
71	WATR04	SW	31.72	115.4	46	42	2	-56	18	66	0	0	57	0	0	-2	0	0	13	14	98
72	BMP120	NSW	36.21	150.32	121	125	14	173	35	-29	1	0	-47	2	1	-3	0	0	38	39	98
73	GBRMYR	CGBR	18.22	147.35	214	190	13	113	17	37	6	2	32	11	3	-11	5	6	91	95	99
74	NRSROT	SW	32	115.42	47	42	1	180	32	59	1	0	78	1	0	-3	0	0	30	31	99
75	SAM7DS	SA	36.2	135.84	519	587	7	150	11	54	1	1	33	2	0	-38	1	1	46	90	99
76	L Musgrave I	SGBR	23.93	152.3	42	42	3	166	5	85	14	2	62	28	4	1	14	14	99	99	99
77	SYD140	NSW	34	151.45	138	144	16	205	27	10	2	1	-20	2	1	42	0	1	22	82	99
78	SYD100	NSW	33.94	151.38	103	117	14	199	26	5	2	1	-18	2	1	39	1	1	36	86	99
79	WACA20	SW	31.98	115.23	199	212	9	168	20	41	0	0	76	0	0	35	0	0	17	67	100
80	WATR50	SW	31.76	114.96	497	469	6	170	15	0	0	0	25	0	0	61	0	0	18	111	100
81	WATR20	SW	31.73	115.04	205	167	16	169	28	11	0	0	47	0	0	66	0	0	32	128	100
82	NRSESP	SW	33.93	121.85	50	44	1	107	5	44	0	0	58	1	0	-18	0	0	95	104	100
83	PH100	NSW	34.12	151.23	110	123	7	224	21	29	1	1	-7	1	1	58	0	1	24	111	101
84	WATR15	SW	31.69	115.13	150	160	10	165	26	-1	0	0	43	0	0	88	0	0	29	160	101
85	SAM4CY	SA	36.53	136.87	117	105	0	-30	22	18	1	0	31	2	1	16	1	1	131	137	101
86	WATR10	SW	31.65	115.2	107	79	9	150	18	-42	0	0	50	0	0	-84	0	1	125	256	102
87	SEQ400	SEQ	27.33	153.88	400	373	28	183	39	-81	1	0	80	2	1	-20	1	2	113	309	104
88	SEQ200	SEQ	27.34	153.77	200	203	23	178	44	-73	1	0	85	3	2	-43	1	4	111	292	105
89	BMP090	NSW	36.19	150.23	91	96	20	172	19	26	1	0	-36	1	0	-138	1	2	89	272	106
90	SAM1DS	SA	36.52	136.24	520	587	5	114	10	-13	0	0	32	1	0	17	1	1	455	460	109
91	NRSNSI	SEQ	27.34	153.56	65	63	25	159	33	83	3	1	85	9	3	-13	6	6	221	225	110
92	Tern I	SGBR	20.85	149.98	47	50	8	141	7	28	22	1	6	32	5	60	11	29	48	131	123
93	ITFTIS	Arnhem	9.818	127.55	464	534	2	223	7	83	8	1	-79	8	2	4	0	16	3	203	154
94	GBRLSL	CGBR	14.34	145.34	330	480	4	-61	12	8	0	0	39	7	1	3	7	7	2395	2395	155
95	NRSNIN	Pilbara	21.87	113.95	61	64	4	211	18	49	7	0	-75	19	-5	6	13	26	195	395	178
mean abs. value	**N=31**				183	191			22		3			5		31	2	4	77	144	105
mean abs. value	**N=95**				106	106			13		32			33		17	6	10	20	33	52

305

Ocean Science
Discussions

EGU
Open Access

Table 4: Tidal major axis velocity and phase region-average statistics, for six constituents (and their root sum of squares).

Velocity major axis amplitude (cm s^{-1})

mean observed amplitude < o >

	Aust	Arnhem	GOC	CGBR	SGBR	SEQ	NSW	Bass	Tas	SA	SW	Pilbara	Kimb.
#sites	95	12	3	5	15	5	6	18	10	9	8	5	7
M2	31.7	69.4	16.3	9.9	31.8	1.8	1.2	66.3	64.1	4.3	0.33	18	35.5
S2	11.3	33	5.3	5.3	12.9	0.44	0.41	10.2	9.1	4.6	0.4	11	21.6
N2	6.1	10.9	3.6	3.2	7.4	0.53	0.37	13.7	13.2	0.41	0.15	3	5.9
K1	6.6	16.3	17.4	2.8	5.3	3.3	3.1	7.3	7.1	5.6	0.72	2.7	4.4
O1	4	9.5	9.7	1.5	2.9	2.6	1.9	5.4	5	3.5	0.53	1.4	2.2
P1	1.6	3.8	0	1.1	1.9	1.1	1.2	1.6	1.6	1.7	0.49	0.62	1
RSS	35.1	80	26.5	12.2	35.7	4.8	4.1	69.1	66.6	9.3	1.1	21.6	42.3

mean magnitude of vector error (MMVE)

	Aust	Arnhem	GOC	CGBR	SGBR	SEQ	NSW	Bass	Tas	SA	SW	Pilbara	Kimb.
#sites	95	12	3	5	15	5	6	18	10	9	8	5	7
M2	10.3	27.4	2.5	5.1	14.7	2.7	1.1	13.9	13.3	1.6	0.3	8.9	8.8
S2	4.6	15.1	2.2	3	5.8	1	0.47	2.7	2.3	1.9	0.54	5.2	6.5
N2	2.2	4.6	0.88	1.7	3.6	0.73	0.27	3.3	3	0.25	0.12	1.6	1.5
K1	4.7	14.8	6.7	1.6	3.8	2.6	3.8	3.7	4.8	2.8	0.82	2.1	2.2
O1	2.8	7	6	0.95	2.4	2.3	2	2.9	3.5	1.7	0.55	1.2	1.3
P1	1.7	3.5	4.6	0.58	1.4	1	1.4	2.3	2	0.85	0.6	0.91	0.98
RSS	12.8	35.8	10.7	6.4	16.9	4.7	4.7	15.4	15.2	4.2	1.3	10.7	11.4
%obs	36.5	44.7	40.3	52.7	47.3	97.7	113.7	22.3	22.8	45.5	114.7	49.8	26.9

mean absolute value of error <|m-o|> (MAE)

	Aust	Arnhem	GOC	CGBR	SGBR	SEQ	NSW	Bass	Tas	SA	SW	Pilbara	Kimb.
#sites	95	12	3	5	15	5	6	18	10	9	8	5	7
M2	6.5	17.3	0.69	4.4	10.2	1.8	0.4	8.5	8	1.1	0.14	5.9	3.1
S2	3	10.5	0.99	2.4	3.7	0.75	0.19	1.9	1.6	1.7	0.15	3.3	1.8
N2	1.3	2.6	0.24	1.5	2.3	0.31	0.098	2.2	2	0.13	0.067	1	0.62
K1	2.3	4.9	3.3	1.1	1.8	2	2.4	2.8	3.1	1.9	0.24	0.53	0.84
O1	1.6	3.1	4.6	0.66	1	2	1.4	2.2	2.2	1.2	0.24	0.47	0.71
P1	1.1	1.3	4.6	0.38	0.69	0.68	0.99	2.1	1.6	0.64	0.26	0.45	0.5
RSS	7.8	21.2	7.4	5.4	11.3	3.5	3	9.9	9.3	3.1	0.48	6.8	3.8
%obs	22.3	26.6	27.9	44.2	31.7	73.3	72.1	14.3	14	33.8	41.7	31.7	9

19

320 **mean error < m-o > (bias)**

	Aust	**Arnhem**	**GOC**	**CGBR**	**SGBR**	**SEQ**	**NSW**	**Bass**	**Tas**	**SA**	**SW**	**Pilbara**	**Kimb.**
#sites	95	12	3	5	15	5	6	18	10	9	8	5	7
M2	1.1	-8.4	0.56	2.1	7.8	1.8	0.4	1	0.61	1	0.14	5.9	1.4
S2	0.49	-1.9	0.99	1.3	3	0.75	0.15	-1.5	-1.3	1.7	0.09	3.3	0.86
N2	-0.05	-1.6	-0.22	0.29	1.5	0.19	-0.064	-0.79	-1	0.096	-0.007	1	-0.26
K1	-0.83	-0.2	-2.1	0.34	0.66	-2	-2.4	-2.2	-3.1	-1.5	-0.000	0.5	0.71
O1	-0.52	0.036	3.7	-0.1	-0.32	-1.9	-1.4	-1.8	-2.1	-0.65	-0.042	0.47	0.71
P1	-0.04	-0.092	4.6	-0.14	-0.21	-0.68	-0.99	-0.02	-0.35	-0.52	-0.26	0.34	0.5
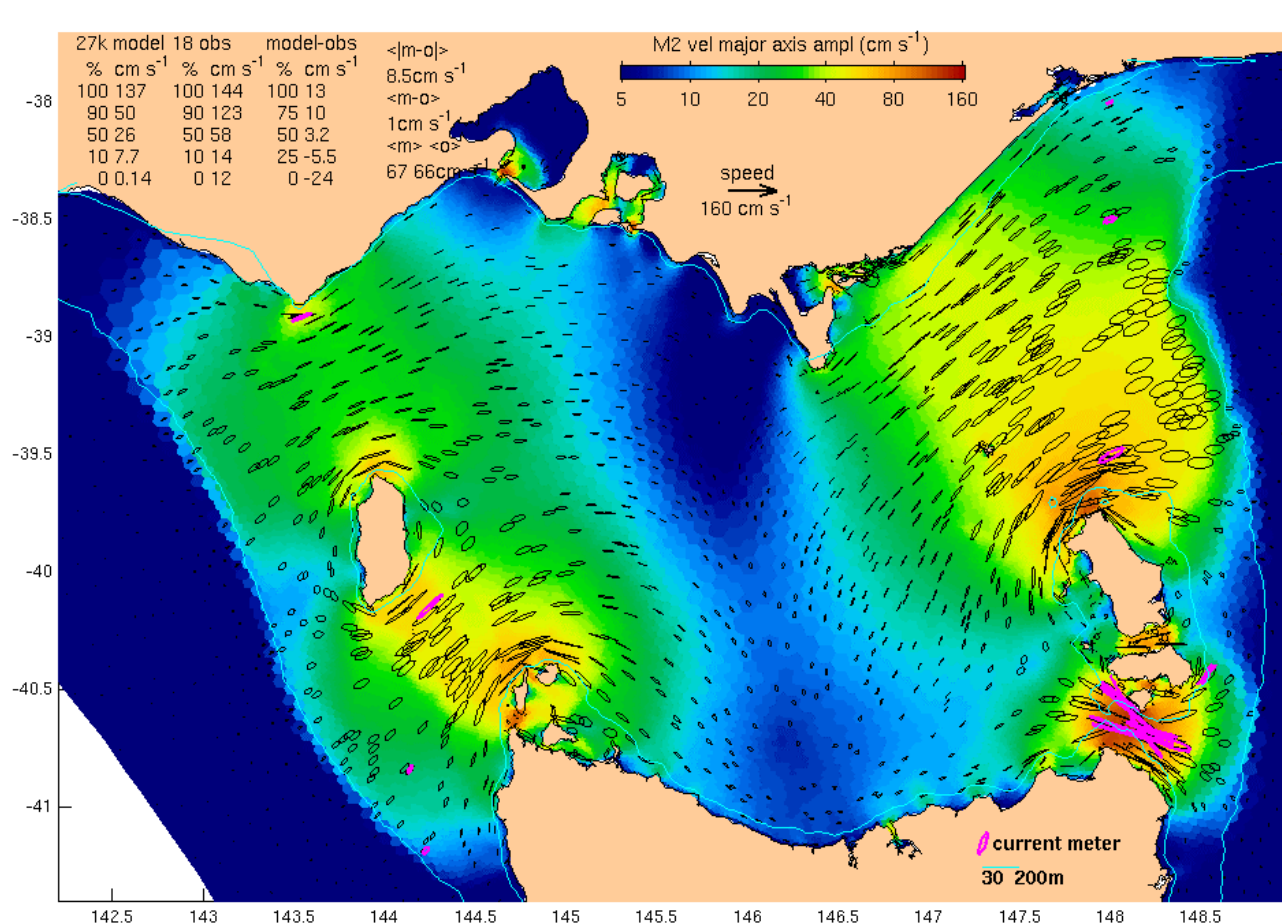
Figure 6 Amplitude of the M2 major axis velocity for Bass Strait, otherwise like Fig. 5, except that percentiles of the model at the locations of the observations are not listed.
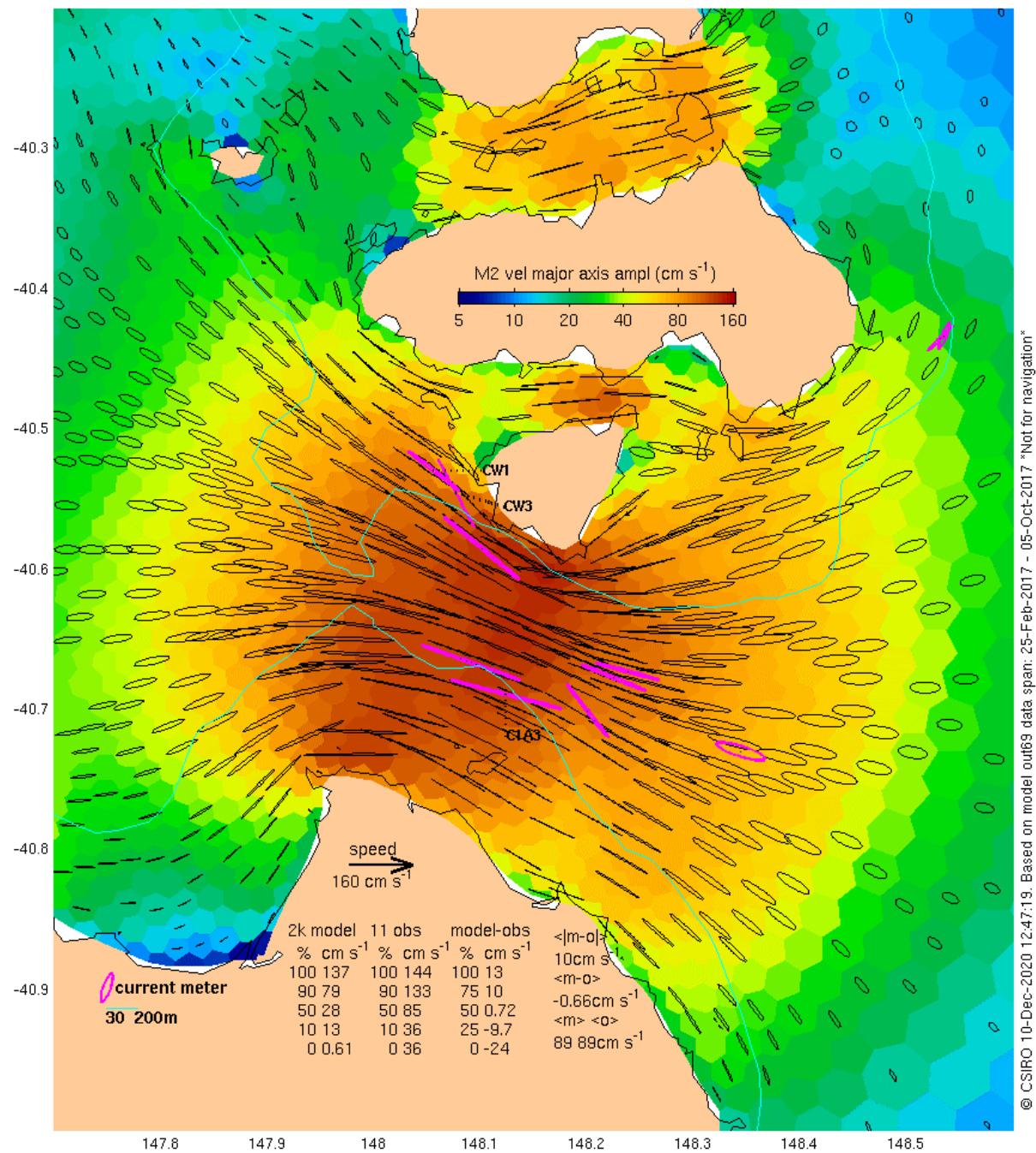
325

Figure 7 Amplitude of the M2 major axis velocity for Banks Strait, otherwise like Fig. 5.

Ocean Science
Discussions

EGU

6.2.1 Bass Strait (including Banks Strait)

The tide comes into Bass Strait from both the east and west, with the strongest flows (Fig. 6) either side of the central basin (see Fig. 2) where the tidal range (Fig. 3) is a maximum. The highest tidal ranges are near Burnie on the northern Tasmanian

330 coast. Recalling that tidal potential forcing is not activated in this run of the model, the agreement of our model with the observations is in contrast with the conclusion by Wijeratne et al. (2012) that tidal potential forcing is required for a nested model of Bass Strait to be accurate. We offer no explanation of this inconsistency. The greatest observed M2 major axis amplitude is 144 cm s^{-1} (at C1A3 in Banks Strait – see Fig. 7, one of the Penesis et al. (2020) ADCPs), where the model estimate is 119 cm s^{-1} (line 19 of Table 3). This is also the biggest error in Bass Strait, but it is still quite a small (17%) relative

335 error. Taking the phase error also into account takes this to 26%. Table 4 lists the M2 MAE across the 18 validation sites in Bass Strait as 8.5 cm s^{-1}. The RSS across 6 constituents is 9.9 cm s^{-1}, or 14.3 % of the 69 cm s^{-1} mean observed RSS of amplitudes – a much better than average (22% across Australia) relative error. Figure 6 and Table 3 show that, across Bass Strait, the modelled M2 current ellipse eccentricities and orientations are mostly in good agreement with observations. The phase errors range from -10° to 12°. Summing over six constituents, and taking the phase errors into account (Table 4), the

340 RSS MMVE is 15.4 cm s^{-1}, or 22.3 % of the mean observed RSS amplitude, making Bass Strait the region with the lowest relative error of RSS MMVE.
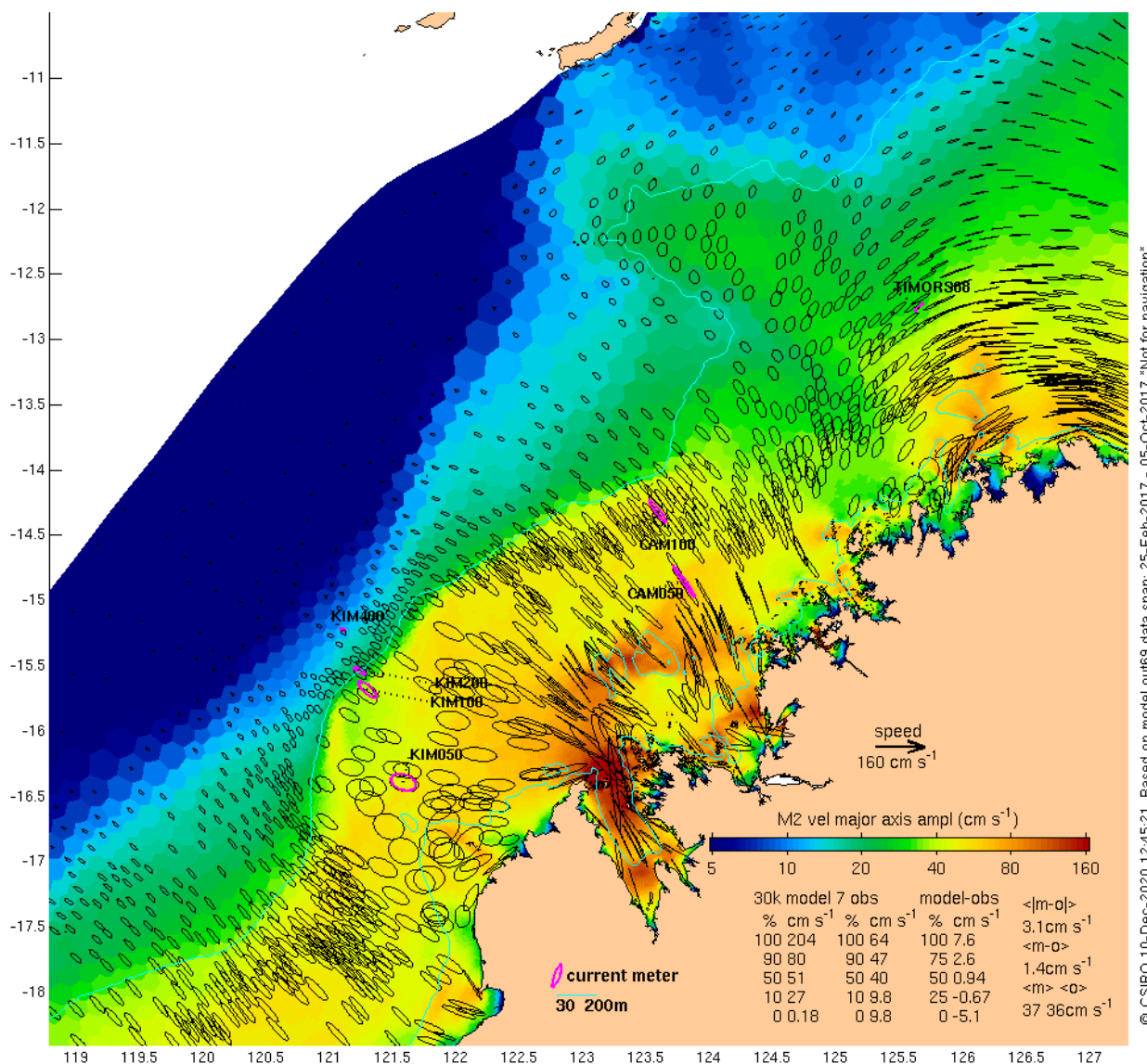
Figure 8 Amplitude of the M2 major axis velocity for the Kimberley, otherwise like Fig. 5.

6.2.2 Kimberley

345   The Kimberley region of Australia includes King Sound, where the greatest tidal range in Australia occurs. The entrance to King Sound has such strong tidal currents that tourists go out to see them in RIBs, helicopters and other vessels. There are not, however, any available instrumental records of the flows in the most energetic regions, so the percentiles of the model (across ~30,000 cells, see Fig. 8) are very different to the percentiles of the observations. Figure 8 shows that the model agrees quite well with the seven available records, including the change from nearly circular M2 ellipses at KIM050 to the shore-normal

350 rectilinear flows at CAM050 and CAM100, and then the shore-parallel ellipses at TIMORS88. The M2 amplitude errors at KIM200 and KIM100 are just 3 and 0 % of the observed amplitude. It is only with the phase taken into account that the M2 relative errors are significant (5 and 12%). The RSS MMVE is 11.4 cm s^{-1}, or 27 % of the observed RSS amplitude, just 5 points higher than the Bass Strait figure.
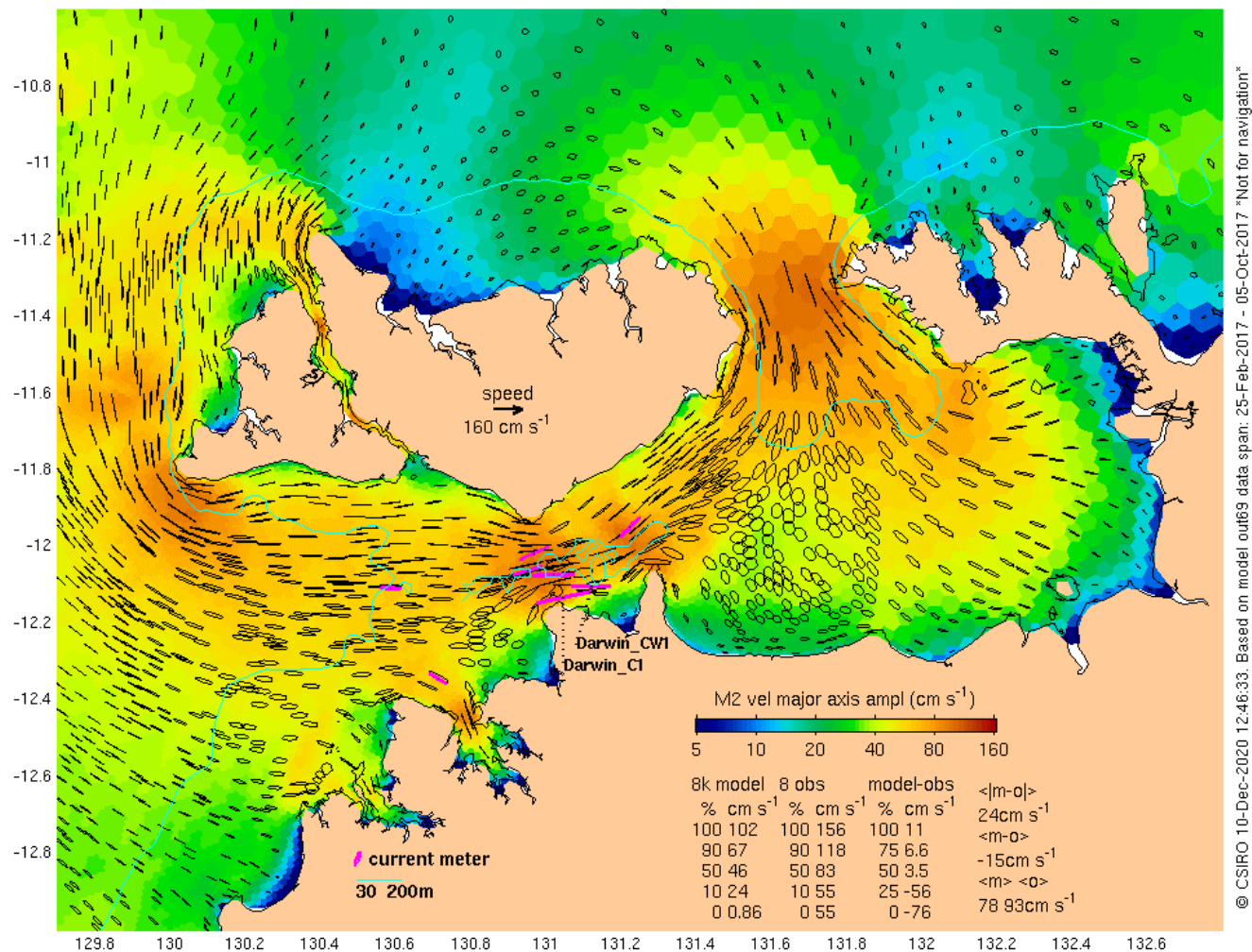
355 **Figure 9 Amplitude of the M2 major axis velocity for the Darwin region, otherwise like Fig. 5.**
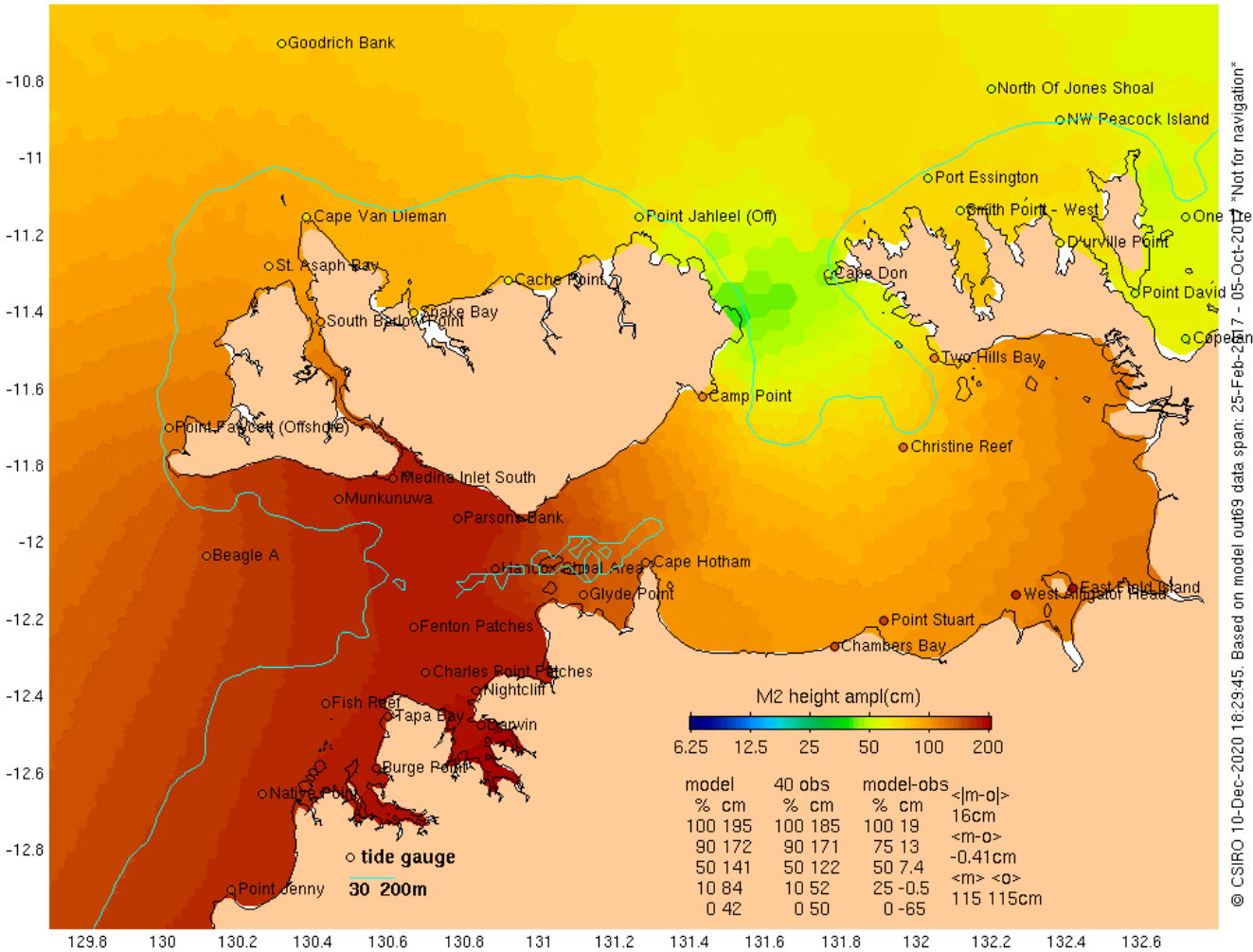
Figure 10 Amplitude of the M2 height for the Darwin region, otherwise like Fig. 3.

6.2.3 Darwin

Figure 9 shows that M2 velocity errors are relatively low at six of the eight sites in the Darwin–Clarence Channel region. Table 3 (lines 46 and 47) identifies the two noticeable exceptions as being the Darwin-CW1 and C1 sites, where the M2 major axis amplitude errors are 56 and 76 cm s^{-1}. At C1 the problem is clearly the topography; model depth is only 8 m but the in situ depth is 52 m. It is less clear why the error at CW1 is large but we will not be surprised if rebuilding the mesh using recently-acquired topography data does not reduce these errors. At present however, the velocity major axis RSS MMVE remains listed as 35.8 cm s^{-1}, or 44.7 % of the observed RSS amplitude. The modelled tidal height amplitude in Van Diemen Gulf (Fig. 10, see Christine Reef for example) is significantly weaker than the observations, for reasons that we are yet to determine.
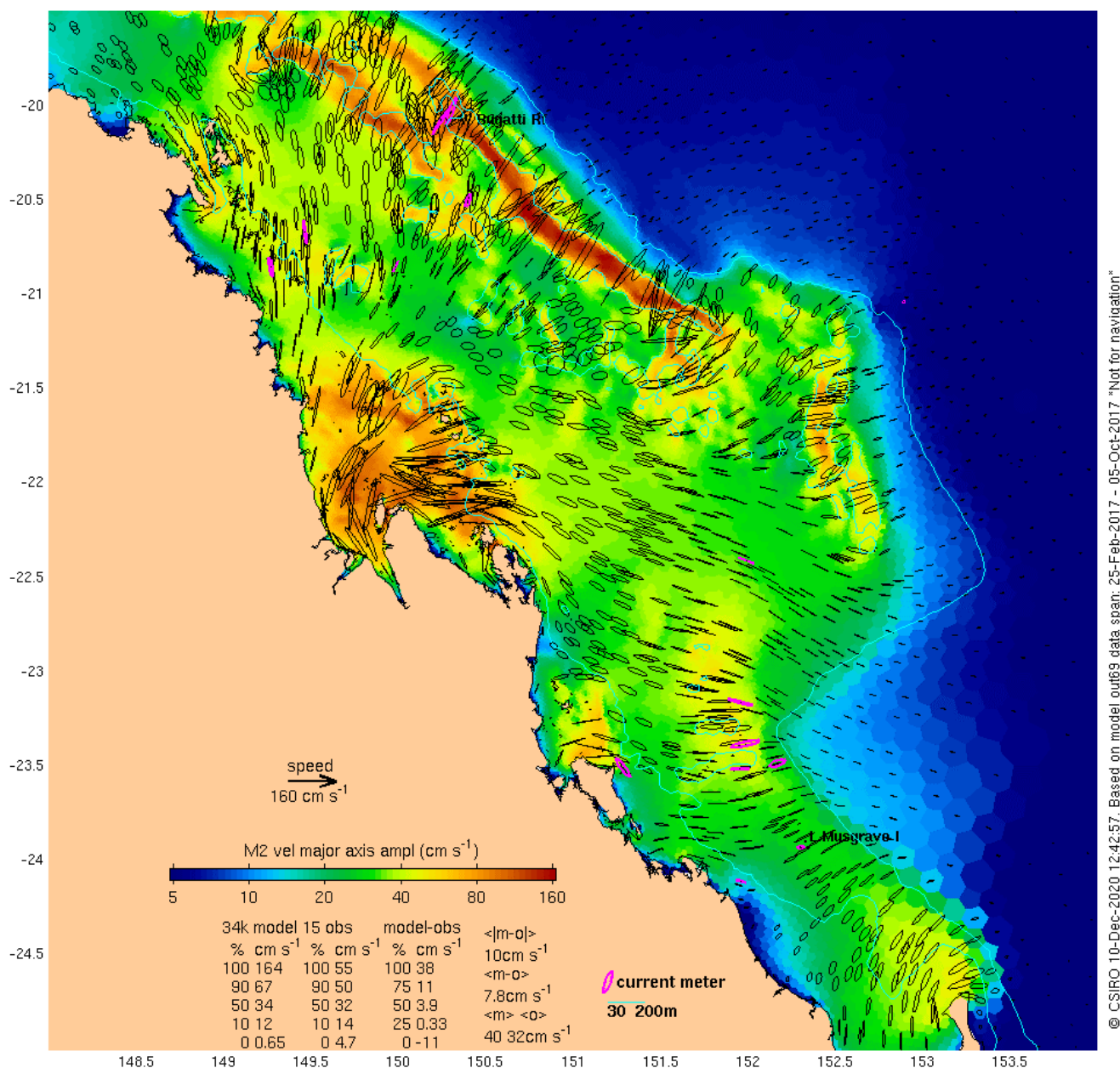
Figure 11 Amplitude of the M2 major axis velocity for the Southern Great Barrier Reef region, otherwise like Fig. 5.

6.2.4 Southern Great Barrier Reef

The Barrier Reef is dense off Broad Sound, causing tides to enter the reef lagoon from both the NW and SE. These waves meet
370   in the lagoon outside Broad Sound then further amplification of the wave entering the Sound occurs due to the geometry of
the Sound (Middleton, Buchwald and Huthnance, 1984). Our model simulates the first process satisfactorily in a qualitative

sense (see Fig. 11), and the modelled and observed tidal currents are in very good agreement at many locations. But Table 4 also lists some large discrepancies at several sites. These are where the observations were made by mechanical current meters, some in topographically complex locations (two near Bugatti Reef, one near Lady Musgrave Island), so the listed RSS MMVE

375 of 16.9 cm s^{-1} (or 47.3 % of the observed amplitude) possibly overstates the true error. The tide gauge (at McEwin Islet) near the head of the Sound (Fig. 3) suggests that the second amplification process is not well modelled, since the modelled range there is only about 75% of the observed range, and the modelled tide lags the observed tide by more than an hour.
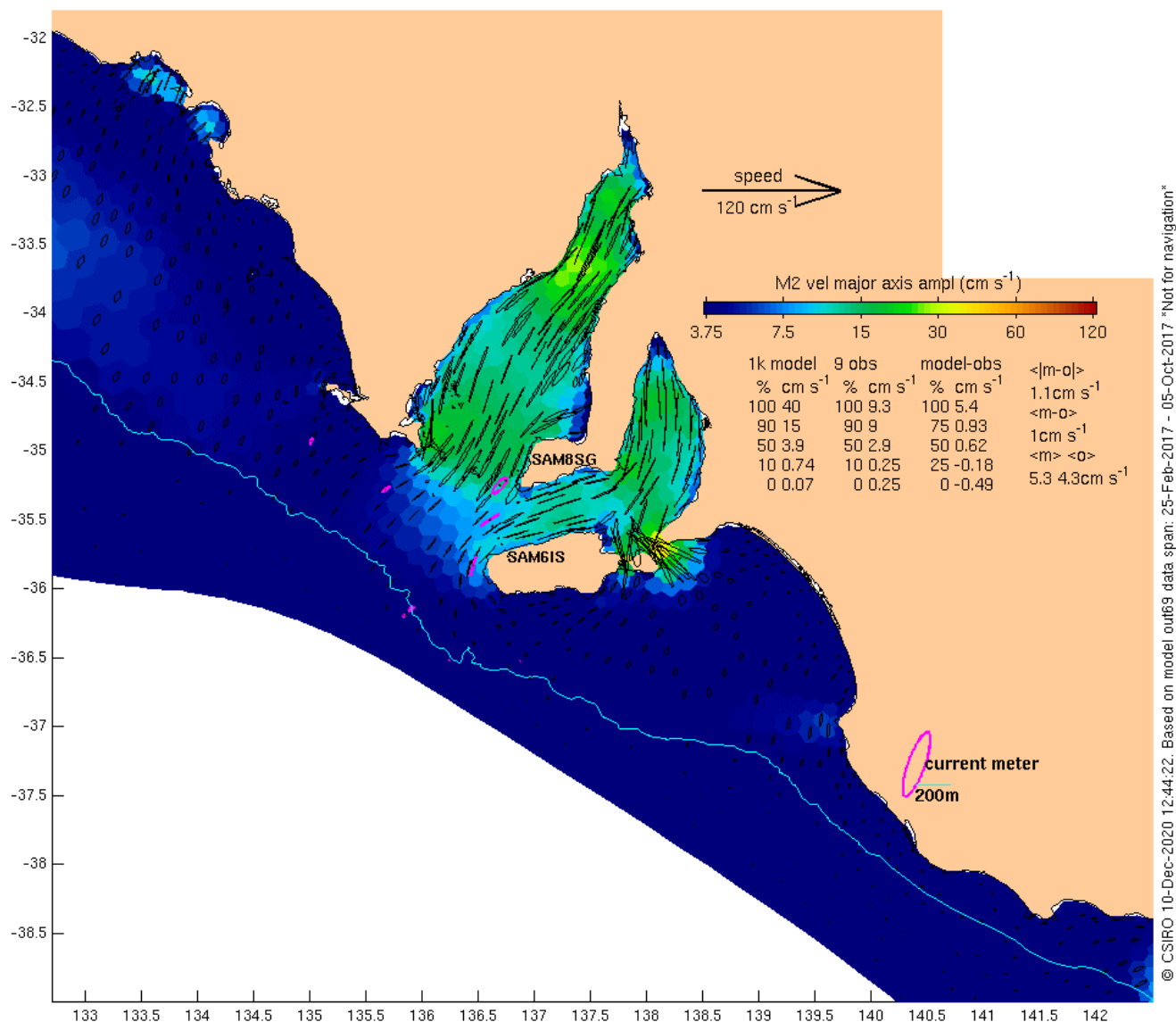
380

Figure 12 Amplitude of the M2 major axis velocity for the South Australia region, otherwise like Fig. 5.

6.2.5 South Australia

A distinctive feature of the tides of South Australia is that the amplitude of S2 exceeds that of M2 (barely), leading to a very strong spring-neap cycle. The vanishing semidiurnal tide on days when M2 and S2 are out of phase is locally known as the

385 Dodge tide. Table 2 lists the SA-average observed M2 and S2 height and major axis amplitudes as 25.6 and 26.7 cm, and 4.3 and 4.6 cm s^{-1}. The model M2 and S2 height and major axis amplitudes (not listed) are also nearly equal, at 23 and 28 cm, and 5.3 and 6.2 cm s^{-1} so Dodge tides will also occur (imperfectly) in model-generated predictions. The maximum modelled M2

major axis amplitude is 40 cm s^{-1} in the South Australian region (Fig. 12), but we have no observations to validate the model at that location. The maximum observed M2 major axis amplitude is 9.3 cm s^{-1} at both SAM6IS and SAM8SG (rows 41 and
390 63 of Table 3) where the model is in very close and moderate agreement, respectively. The RSS MMVE is 4.2 cm s^{-1}, or 45.5 % of the observed amplitude.

6.2.6 Pilbara

Table 3 lists results for just five sites in the Pilbara region (one being the Ningaloo site mentioned earlier as having the greatest error). Unfortunately, these are all we have in our validation dataset despite the economic importance of marine traffic in this
395 region. Results for the three IMOS ADCPs near 20° S (PIL050, 100 and 200) include M2 vector errors of 7 to 25 % of the observed amplitude. But this region is well known for strong internal tides (Book et al., 2016), to which our analysis method is essentially blind, and thus underestimates the errors. Internal tides aside, the RSS MMVE for this region is 10.7 cm s^{-1}, or 49.8 % of the observed amplitude.

6.2.7 Gulf of Carpentaria, Torres Strait, Central Great Barrier Reef

400 The GOC and CGBR regions have intermediate (40.3 and 52.7 %) relative errors of the RSS MMVE, but being based on just 3 and 5 sites, these statistics are uncertain. Nevertheless, we see value in publishing tidal current predictions for these two regions, with appropriate warnings, partly because the sub-tidal currents are weak in these two regions. As mentioned earlier, Torres Strait is one of the few places where official tidal current predictions are already published. We have not yet compared those predictions, or observation-based constituents with our model.

405 ### 6.2.8 South-east Queensland, New South Wales and South West

The relative error of the RSS MMVE for the SEQ, NSW and SW regions are 98, 114 and 115 %, respectively, suggesting that the model is not simulating the tidal currents in these regions very well, even though it is simulating the heights (recall that NSW is one of the regions with the lowest relative error of height). These narrow-shelf regions are also where the sub-tidal currents (Table 3) far exceed the tidal currents, so predictions of tidal currents would be of limited practical value even if they
410 were accurate. For both these reasons, we will not be publishing tidal current predictions from the COMPAS model for these regions.

7 Discussion

We have evaluated the tidal heights in our COMPAS model against a large number (615) of sites around Australia, giving a much more detailed picture than was given, for example, by Haigh et al. (2014) or Seifi et al. (2019), while being broadly
415 consistent. But modelling tidal heights is not the principal motivation of this study. Our focus is on tidal currents (depth-averaged at this point), about which much less has been written (Stammer et al., 2014; Timko et al., 2013). Lyard et al. (2020)

compare FES2014 with the same IMOS data we have used (just graphically). They conclude that for shelf currents, there is still a need for nested regional models (such as ours), with finer grids than global models have.

We have shown that our COMPAS model of the barotropic tide is in very good agreement with observed tidal currents at
420 many, but certainly not all, of the 95 sites at which we have in situ validation data. A large number of the sites with high relative errors are where the tides are very weak, so it could be argued that those errors are of little practical interest. Over the continental shelf, this is the case for the southern half of the continent from Ningaloo Reef in the west to Fraser Island in the east, excepting Bass Strait and the South Australian gulfs (i.e. the sections where the shelf is narrow). This leaves 79 % by area of Australia's shelf waters as being where tidal currents are both predictable and a significant proportion of the total
425 variance. Bass Strait and the Kimberley region are where our model performs best, with the root sum of square (across 6 constituents), regional-average vector error of the major axis velocity being less than 27% of the observed signal. This measure of the relative error of the model's tidal predictions is between 40 and 50 % in the other regions where we think the predictions should be made available to the public.

We hope to expand our tidal currents validation dataset, especially at locations (mainly in the NW) where observations have
430 been made by offshore industries, in order to guide development of the next version of our model. Incomplete as it is, we are publishing it now along with the output of our model because we are sure it will have enduring value, for example, to developers of global models such as Lyard et al (2020) who used a preliminary version of the validation dataset.

It is well established (e.g. by Ray et al., 2011) that accurate topography is an essential component of a good tidal model and our results and those of Sahuc et al. (2020) bear this out. Some of the largest model errors are where there is a big discrepancy
435 between the depth in the model and the depth that was recorded on site during mooring deployment. Improving the topography in our model is certainly a priority for future model development. This will likely comprise a combination of inverse tuning where local bathymetry alterations are made to optimally correlate model predictions to observation, and capitalising on the results of the ausSeabed initiative (http://www.ausseabed.gov.au/about).

Boundary conditions are also, of course, an essential input for a regional tidal model. We have only tested our model using
440 open boundary forcing from TPXO9v1, but hope to test it soon using TPXO9v2 and FES2020.

8 Conclusions

We have shown that for many regions around Australia's continental shelf, our model can predict depth-averaged tidal currents with enough accuracy to arguably be operationally useful for mariners and maritime industries. Regions where tidal currents are most predictable and in excess of non-tidal currents include Bass Strait, the Kimberley, Joseph Bonaparte Gulf to Arnhem
445 Land and the southern Great Barrier Reef. Consequently, these are the regions for which we intend to commence publishing 'unofficial' predictions of tidal currents (both model-based and observation-based). They are also the regions of greatest interest to the renewable energy sector, for whom we have published maps based on the model discussed here. We intend also to publish tidal current predictions for the South Australian gulfs, the Pilbara, Gulf of Carpentaria, Torres Strait and the central

Ocean Science
Discussions

and northern Great Barrier Reef regions but with a warning that there may be greater errors in these regions. For the rest of
450 Australia (comprising the narrow-shelf regions of the southern half of the continent) we see no need to publish tidal current
predictions, largely because the non-tidal currents are dominant.

9 Code Availability

COMPAS is supported by CSIRO, Australia and available open source at https://github.com/csiro-coasts/EMS, with
documentation provided at https://research.csiro.au/cem/software/ems/ems-documentation/. We appreciate the encouragement
455 of the MPAS developers in pursuing this work.

10 Data availability

- Three project data sets have been published by Herzfeld, et al. (2020) https://doi.org/10.25919/nqdc-1v40 :
    1. The first 59 of the 222 days of COMPAS output hourly time series, at all cell centers, for all state variables
    2. harmonic constituents of the COMPAS velocity and height fields, derived from a 222 day model run so K1 and
460   P1 are resolved
    3. harmonic constituents of the currents validation dataset, along with subtidal ellipse parameters for 95 locations.
- COMPAS-based estimates of Australia's tidal energy resource are available at
    1. https://nationalmap.gov.au/renewables/
- Current meter validation dataset timeseries are available at: https://portal.aodn.org.au/
465 - Graphics similar to the Figures in this paper showing constituents other than M2, other regions, other variables, and
    statistical properties of the tidal heights, energy fluxes, etc. http://www.marine.csiro.au/~griffin/ARENA_tides/tides/

Author contribution

David Griffin assembled the validation data set, performed the model-data comparisons and prepared the manuscript, with
contributions from coauthors. Mike Herzfeld developed and ran the COMPAS model. Mark Hemer led the main (ARENA)
470 project that this study is part of, contributed to the analyses and maintained linkages with collaborators.

Competing interests

The authors declare that they have no conflict of interest.

Disclaimer

The data products of this research are not for navigation. The work is only a step towards an operational product.

Ocean Science
Discussions

References

Beaman, R. J.: Project 3DGBR: A high-resolution depth model for the Great Barrier Reef and Coral Sea, Marine and Tropical Sciences Research Facility (MTSRF) Project 2.5i.1a Final Report, Reef and Rainforest Research Centre, Cairns, Australia, 13pp, 2010.

Book, J. W., Jones, N., Lowe, R., Ivey, G., Steinberg, C. R., Brinkman, R. M., Rice, A. E., Bluteau, C., Smith, S. R., Smith, T. A., and Matt, S.: Propagation of internal tides on the Northwest Australian Shelf studied with time-augmented empirical orthogonal functions, in: Proceedings of the 20th Australasian Fluid Mechanics Conference, Perth, Australia, 5–8 December 2016, http://people.eng.unimelb.edu.au/imarusic/proceedings/20/744%20Paper.pdf, 2016.

Codiga, D.L.: Unified tidal analysis and prediction using the UTide Matlab functions, Technical Report 2011-01, Graduate School of Oceanography, University of Rhode Island, Narragansett, RI, 59pp, ftp://www.po.gso.uri.edu/pub/downloads/codiga/pubs/2011Codiga-UTide-Report.pdf, 2011.

Egbert, G.D. and Erofeeva, S.Y.: Efficient inverse modelling of barotropic ocean tides, J. Atmos. Oceanic Technol., 19(2), 183–204, doi: 10.1175/1520-0426(2002)019<0183:EIMOBO>2.0.CO;2, 2002.

Engwirda, D.: JIGSAW(GEO) 1.0: locally-orthogonal staggered unstructured grid generation for general circulation modelling on the sphere, Geosci. Model Dev., 10 (6), 2117–2140, doi: 10.5194/gmd-10-2117-2017, 2017.

Griffin, D. A., Middleton, J. H. and Bode, L.: The tidal and longer period circulation of Capricornia, southern Great Barrier Reef, Aust. J. Mar. Freshwater Res., 38, 461–474, 1987.

Ocean Science
Discussions

Open Access

EGU

Haigh, I. D., Wijeratne, E. M. S., MacPherson, L. R., Pattiaratchi, C. B., Mason, M. S., Crompton, R. P., and George, S.: Estimating present day extreme total water level exceedance probabilities around the coastline of Australia: tides, extra-tropical storm surges and mean sea level, Climate Dynamics, 42, 121–138, doi: 10.1007/s00382-012-1652-1, 2014.

Herzfeld, M.: An alternative coordinate system for solving finite difference ocean models, Ocean Modelling, 14 (3–4), 174–196, doi: 10.1016/j.ocemod.2006.04.0022006, 2006.

Herzfeld, M., Engwirda, D., and Rizwi, F.: A coastal unstructured model using Voronoi meshes and C-grid staggering, Ocean Modelling, 148, doi: 10.1016/j.ocemod.2020.101599, 2020.

Herzfeld, Mike; Griffin, David; Hemer, Mark; Rosebrock, Uwe; Rizwi, Farhan; Trenham, Claire (2020): AusTEN National Tidal model data. v2. CSIRO. Data Collection. https://doi.org/10.25919/nqdc-1v40 .

Lyard, F. H., Allain, D. J., Cancet, M., Carrère, L., and Picot, N.: FES2014 global ocean tides atlas: design and performances, Ocean Sci. Discuss., doi: 10.5194/os-2020-96, in review, 2020.

Middleton, J.H., Buchwald V.T. and Huthnance, J.M.: The anomalous tides near Broad Sound, Continental Shelf Research 3, 359–381, doi: 10.1016/0278-4343(84)90017-7, 1984.

Pawlowicz R., Beardsley, B. and Lentz, S.: Classical tidal harmonic analysis including error estimates in MATLAB using T_TIDE, Computers and Geosciences 28, 929–937, doi: 10.1016/S0098-3004(02)00013-4, 2002.

Penesis, I., Hemer, M., Cossu, R., Nader, J. R., Marsh, P., Couzi, C., Hayward, J., Sayeef, S., Osman, P., Rosebrock, U., Grinham. A., Herzfeld, M. and Griffin, D.: Tidal Energy in Australia: Assessing Resource and Feasibility in Australia's Future Energy Mix, Australian Maritime College, University of Tasmania, 2020.

Ray, R. D., Egbert, G. D. and Erofeeva S. Y.: Tide predictions in shelf and coastal waters – status and prospects, in: Coastal Altimetry, edited by: Vignudelli, S., Kostianoy, A. G., Cipollini, P. and Benveniste, J., Springer-Verlag, Berlin, Germany, 191–216, 2011.

Ringler, T. D., Thuburn, J., Klemp J. B. and Skamarock, W. C.: A unified approach to energy conservation and potential vorticity dynamics on arbitrarily structured C-grids, J. Comput. Phys., 229 (9), doi: 10.1016/j.jcp.2009.12.007, 2010.

Sahuc, E., Cancet, M., Fouchet, E., Lyard F., Dibarboure, G. and Picot, N.: Bathymetry Improvement and High Resolution Tidal Modelling around Australia, Ocean Surface Topography Science Team meeting, October 20-23, 2020.

Seifi, F., Deng, X., Andersen, O. B.: Assessment of the accuracy of recent empirical and assimilated tidal models for the Great Barrier Reef, Australia, using satellite and coastal data, Remote Sens., 11, 1211, doi: 10.3390/rs11101211, 2019.

Stammer, D., Ray, R. D., Andersen, O. B., Arbic, B. K., Bosch, W., Carrère, L., Cheng, Y., Chinn, D. S., Dushaw, B. D., Egbert, G. D., Erofeeva, S. Y., Fok, H. S., Green, J. A. M., Griffiths, S., King, M. A., Lapin, V., Lemoine, F. G., Luthcke, S. B., Lyard, F., Morison, J., Müller, M., Padman, L., Richman, J. G., Shriver, J. F., Shum, C. K., Taguchi, E. and Yi, Y.: Accuracy assessment of global barotropic ocean tide models, Rev. Geophys., 52, 243–282, doi:10.1002/2014RG000450, 2014.

Thuburn, J., Ringler, T. D., Skamarock, W. C. and Klemp, J. B.: Numerical representation of geostrophic modes on arbitrarily structured C-grids, J. Comput. Phys., 228 (22), 8321–8335, doi: 10.1016/j.jcp.2009.08.006, 2009.

Ocean Science
Discussions

Open Access

Timko, P. G., Arbic, B. K., Richman, J. G., Scott, R. B., Metzger, E. J. and Wallcraft, A. J.: Skill testing a three-dimensional
540 global tide model to historical current meter records, J. Geophys. Res.: Oceans, 118, 6914–6933, doi: 10.1002/2013JC009071,
2013.

Wijeratne, E. M. S., Pattiaratchi, C. B., Eliot, M. and Haigh, I. D.: Tidal characteristics in Bass Strait, south-east Australia,
Estuarine, Coastal Shelf Sci., 114, 156–165, doi: 10.1016/j.ecss.2012.08.027, 2012.

545 **Figure Captions**

565